Diffusion in Molten Metals and Metalloids

by

Josée Robert

•

A thesis submitted to the Department of Materials and Metallurgical Engineering

in conformity with the requirements for

the degree of Master of Science (Engineering)

Queen's University

Kingston, Ontario, Canada

May, 1999

Abstract

The present work was motivated by the need for accurate diffusion data for the study of metallurgical processes. In addition, it will help in obtaining a better understanding of the mechanism(s) of diffusion and the structure of liquids which, in time, should permit the prediction of diffusion data for a given materials system. There are many theories, each giving a different equation, to describe the temperature dependence of the diffusion coefficient. This relation is of practical and theoretical importance and cannot be distinguished by terrestrial experimental results because of poor reproducibility, primarily due to the influence of buoyancy-driven convection. It is demonstrated that with the experience of recent experimental techniques in space, it is possible to avoid convection and hence, permit the use of the space laboratory as a near-ideal environment for the study of liquid diffusion.

Long capillary liquid diffusion couples of five alloy systems, namely Pb-Au, Pb-Ag, Sb-In, In-Sb, and Pb-Sb, were isothermally processed at a series of temperatures on the MIR Space Station using the QUELD II furnace facility, coupled to the Canadian Microgravity Isolation Mount (MIM). The MIM provides the opportunity for 1) exposing the diffusion couples to the ambient g-jitter of MIR, 2) isolating them from this and also 3) subjecting them to a forcing vibration superimposed on the isolating state. The results obtained will be described and reviewed with respect to existing models of diffusion in liquids.

Acknowledgements

I would like to start by thanking my supervisor, Dr Smith, for his support and guidance throughout this study and his patience when coping with my repeated phrase "just one more question Dr Smith".

I would also like to express my gratitude to Dr Charlie Zhu for advice concerning sample preparation and analysis. Invaluable assistance from Dr John Page and the Analytical Services Unit regarding AAS analysis is much appreciated. For all their help, encouragement, and patience, I would like to thank my family, friends, and colleagues, technicians and staff of the Materials and Metallurgical Engineering Department.

My gratitude goes out to the Canadian Space Agency and Millenium Biologix Inc. for providing endless assistance and support whenever necessary. Their valuable help is greatly appreciated.

Finally, I would like to acknowledge NSERC and Queen's University, for providing funding and support for this research project.

Table of Contents

List of Figures

List of Tables

List of Symbols

A	absorbance
A	area crossed by the diffusion path
A	system constant
A^l	system constant
a^*	jump distance
b	lightpath
b	system constant
C	concentration
C_o	initial concentration
d	initial length of the alloy part of the diffusion couple
D	diffusion coefficient
D_o	system constant
D^E_i	binary collision D of the solute in the solvent
ε	molar absorptivity
g	geometric factor
γ	numerical factor
$g_{is}(\sigma_{is})$	radial distribution function of unlike atoms at contact
η	viscosity
i	solute
is	mixture of the binary solution
J_T	total flux
k	Boltzmann constant
K	force constant
μ	mobility of the diffusing species
μ	reduced mass
N	Avogadro's number
Q	activation enthalpy of diffusion
R	gas constant
R	radius of spherical particles
s	solvent
σ	hard-sphere diameters
t	diffusion time
T	temperature
u	gas kinetic velocity
V_f	free volume of the liquid
V^*	critical volume associated with the diffusing atom
x	diffusion distance
x_o	maximum diffusive displacement
Z	specified liquid state coordination number

1 Introduction

1.1 History of the Project

In 1983, Professor Reginald Smith, the PI (principal investigator) in this MIR project, completed successfully in a National Research Council of Canada competition to design an experiment worthy of support as a Get-Away-Special project (GAS-can). From this, Queen's University Experiments in Science and Technology in Space (QUESTS) was born. However, the NASA STS Challenger disaster forced an extended delay and, as a result, QUESTS I finally flew with 12 diffusion experiments in 1992 and again (QUESTS II) in 1994. This was followed by Queen's University Experiments in Liquid Diffusion (QUELD I), an STS Mid-deck experiment conceived in 1984 and designed as part of the 2nd Canadian Space Experiments (CANEX 2) associated with the flight of Dr Steve MacLean on STS-52. During the flight Dr Steve MacLean and his associates on Columbia processed 36 diffusion samples by manually feeding samples into two compact isothermal furnaces with attached quenching devices.[1]

With its development of MIM, the Canadian Space Agency selected a number of materials processing systems to be mounted on MIM (Microgravity Isolation Mount) for a projected MIR/MIM extended mission. QUELD II is one of these and has now been operating on MIR for more than two years and has processed approximately 200 samples, including 150 diffusion samples.[1]

QUELD II is the semi-automated version of QUELD I, the operator still being required to manually load the furnaces. Details of this facility are given in Appendix I.[2] For its two processing channels, QUELD II uses a variant of the space-proven

three zone furnace and quench system designed for QUESTS and QUELD I. QUELD II is designed to operate with MIM as its physical and services support platform (Appendices I and II). The astronaut/cosmonaut time involved in the loading/reloading of samples is minimal (2-3 minutes), since the processing variables are introduced via a multi-sample ROM data card inserted in to QUELD II when starting a new batch of samples.[1]

1.2 Liquid Diffusion

Diffusion in liquid metals is of fundamental importance in studying and modelling metallurgical processes. For instance, the solidification of an alloy from its melt involves the redistribution of alloying elements. This, in turn, involves the diffusion of solute species. In order to achieve optimum control of commercial casting processes such as those involved in continuous casting, it is necessary to develop a numerical control model, for which accurate diffusion data are required. Currently available data, where it exists, are often widely inaccurate. The published values for any particular value of the liquid metal diffusion coefficient differ by 50-100%. This is primarily due to the influence of buoyancy-driven convection on the experimental systems used to obtain the coefficients.[3] Most of these experiments have used the long capillary diffusion couple. It is found that the reproducibility of liquid diffusion coefficients measured in a terrestrial laboratory, i.e., at 1g, is poor due to the intrinsic diffusive transport being enhanced by this uncontrolled buoyancy convection since it is well known that this gravity-driven convection can provide a large contribution to the transport of mass in liquid metals.

Even though great efforts have been made in the past decades to minimize buoyancy effects, it is still difficult to produce accurate experimental data in the terrestrial laboratory. Microgravity can offer an environment without significant buoyancy problems and so permit the capture of more precise diffusion data.

However, the influence of the ever-present transient accelerations due to momentum changes (g-jitter) on a space platform needs to be taken into consideration. Recently, the Canadian Space Agency has developed a MIM for use on space platforms in low earth orbit, (see Appendix II[4]). This facility may be used in three modes:

1) "Latched" in which the so-called "flotor", the platform to which the experiment is strapped, is rigidly attached to the "stator" containing the magnetic levitation devices and control computer;
2) "Isolating" in which g-jitter is attenuated; and
3) "Forcing" in which a selected forced oscillation is superimposed upon the isolating condition.

The use of the MIM in the isolating mode reduces the effect of g-jitter on the measured value of diffusion coefficients. The use of MIM in forcing mode permits the correlation of fluid dynamics predictions with the physical consequences of the actual g-jitter experienced by the sample and hence can be used to refine the theory. This is of crucial importance at the current time in view of the need to fine-tune the calculations used to examine the effects of design variants of the International Space Station Alpha (ISSSA) on potential g-jitter.

1.3 Objectives

This liquid diffusion program has been in progress since 1983 and many individuals have contributed to its progress. The objectives of the experiments conducted to-date were to:

i) Measure the diffusion coefficient values for selected molten metals and semiconductors at various temperatures;

ii) Derive i) for MIM in latched mode (raw g-jitter), MIM in isolated mode (minimized g-jitter), and MIM in forcing mode (inducing predictable fluid transport);

iii) To use the data from i) and ii) to refine the theory of the structure of liquids, to predict diffusion coefficient values for liquid systems of scientific and commercial interest in normal and reduced gravity fused media processing.

The work carried-out for this thesis includes:

a) the inspection of the as-received flight samples,

b) the development of high accuracy chemical analysis procedures,

c) the carefully sectioning of ductile and brittle specimens,

d) the chemical analysis of specimens,

e) the compilation and correlation of experimental data to provide diffusion coefficients; and

f) a comparison of these experimental data with theoretical predictions.

2 Background

2.1 Preface

In order to reduce convective transport, the diameters of the capillaries have been progressively decreased, see Figure 1. However, it has been reported that if the diffusion capillary is less than about 1 mm diameter, then the rate of diffusion (D) is reduced.[5] Thus it is conventional to write:

$$D_{effective} = D_{intrinsic} + D_{buoyancy} + D_{wall\ effect} + D_{thermal\ (Sorêt\ effect)}$$

where $D_{intrinsic}$ is due to the atomic diffusion only, $D_{buoyancy}$ is the contribution of macroconvection, $D_{wall\ effect}$ and $D_{thermal}$ are the contributions from the capillary container wall and the thermal gradient, respectively. It has been supposed that if a diffusion couple is isothermally processed in microgravity, then $D_{buoyancy}$ and $D_{thermal}$ will be absent and so only $D_{intrinsic}$ and $D_{wall\ effect}$ should be present. By choosing capillaries of different diameters, an estimate of $D_{wall\ effect}$ might be made and hence an accurate value of $D_{intrinsic}$ could be obtained. Further, if the diffusion couples are processed at a number of temperatures, the temperature dependence of the transport process taking place could be determined. This can provide clues to the mechanism(s) by which diffusion occurs.

2.2 Convection

In liquid diffusion measurements in a terrestrial laboratory (at 1g), the total mixing is due to several contributions, one of them being atomic diffusion. The analysis is then misleading in believing that the concentration profiles are a product

of atomic diffusion only. As a consequence, the measured values suffer from large inaccuracies.

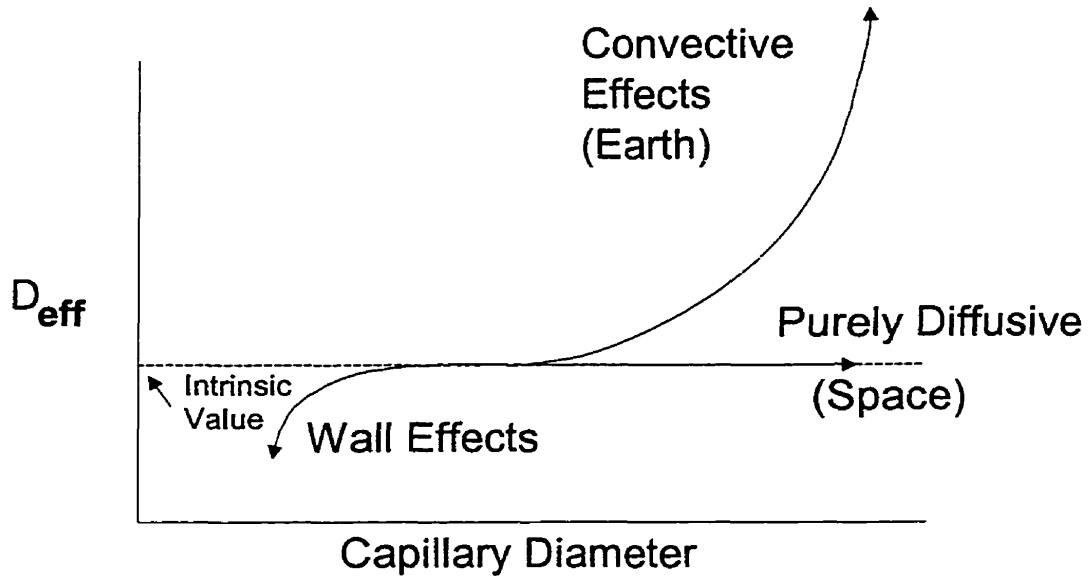

Figure 1 Influence of Buoyancy on the Diffusion Coefficient

2.2.1 Macroconvection and Microconvection

Macroconvections are produced by gravity-driven convections as a result of density gradients which are usually caused by temperature and concentration gradients. Macroconvection normally results in typical deformations of the concentration profile, whereas microconvection and weak laminar convection contribute to the mass transport in fluids similar to diffusion. It is, therefore, almost impossible to separate the two.[6] As mentioned in the preface, reducing the diameter of the capillary minimizes the effects of macroconvection.

Since temperature and concentration gradients produce gravity-convection on the ground, the investigators have generally overlooked the existence of similar types of convection, produced by the same gradients but as a result of surface tension

variations. It was one of the unforeseen results of space experiments which showed the importance of Marangoni convection in diffusion experiments.[7]

2.2.2 Marangoni Convection

Marangoni convection, also known as thermocapillary convection, is a gravity-independent type of natural convection. This type of convection occurs in liquids with free surfaces if there is a gradient of surface tension along the melt surface, such gradients can result from changes in surface temperature or composition. There is no activation barrier to be overcome and minute temperature gradients ("isothermal conditions") suffice for the onset of flow.[6]

If an interface tension gradient is present along the surface of a liquid or along the interface of two liquids, then a shear force arises from regions with low interface tension to regions with high interface tension. Differences in temperatures and concentrations may cause this gradient in the interface tension.[8] Thus, in any attempt to obtain accurate diffusion coefficient values, Marangoni convection may be quite detrimental, especially when the experiment extends over a long period.

Therefore, when considering Marangoni convection, it is important to eliminate free surfaces from test samples, in particular, in the diffusion zone and when steep thermal gradients are used. However, the use of crucibles with smaller diameters can contribute to a decrease in the contribution to the mass transport by Marangoni convection. Hence, this type of convection tends to be negligible in a well designed isothermal experiment.

It is now doubtful whether the wall effects, often reported in the diffusion literature, really exist and originate from a damping of atom movements near the

capillary wall; perhaps the experimental results were associated with a reduction of Marangoni convection as the capillary size decreased.

2.2.3 Wall Effects

Analogous to surface and interface diffusion in solids, wall effects, should they exist, would result in a reduced diffusion transport in the immediate neighbourhood of the capillary wall. This was reported as a result of the practice of using smaller diameter capillaries to study liquid diffusion, thus increasing the wall to cross-sectional area ratio of the wall of the capillary and the liquid channel.

According to the limited experimental work done on the wall effect, it would appear that the wall effect primarily depends upon the interaction between the capillary material and the material of the diffusion couple, (the metal in this study).[9] Self-diffusion experiments in tin with capillary diameters of 1 and 3 mm obtained only minor differences.[5]

It is still not clear if the wall effect exists since, no satisfactory results have been yet reported in the literature to determining its extent.[6]

In order to reduce "wall effect", a larger diameter specimen is necessary whereas to decrease the Marangoni convection, a smaller diameter is needed. Unfortunately, it seems that more attention has been drawn to wall effect than to Marangoni convection; however, the results from the space experiments indicate that Marangoni convection effects are a more serious problem in space. For these reasons, a small diameter diffusion couple was chosen for this study.

2.2.4 Sorêt Effect

Sorêt effect, also known as thermal diffusion in liquids, arises from the relative motion of the components of a solution due to a temperature gradient within the solution. It is observed in solid, liquid, and gaseous multicomponent systems.[10]

If an imposed temperature gradient causes chemical potential gradients for some of the components, diffusion can occur even in an initially uniform system. The Gibbs function of the system will be reduced as a consequence of developing mass flow and concentration gradients. The separating effect of thermal diffusion will be balanced by the remixing effect of concentration-dominated diffusion when a steady state is reached.

In the case of binary systems at elevated temperatures, one can observe that the lighter molecules are concentrated at the hotter end of the temperature gradient while the heavier ones are at the colder end. The separation effect increases with the mass ratio between the molecules.

2.2.5 Summary

All of the above design requirements were respected when the liquid diffusion experiments were performed. To reduce macroconvection, capillary tubes with small diameters were used. Graphite was found to have no significant reaction with the alloys used and could be easily machined. Since it was also a good thermal conductor, its use was beneficial in reducing Sorêt convection. Boron nitride could have been used but was not due to cost and availability. Furthermore, to avoid Marangoni convection, a spring-loaded capillary end cap was used to permit the

volume changes during melting and solidification without the generation of any free surface between the melt and the crucible.

2.3 Theories and Models of Diffusion Mechanism(s) in Liquids

One of the most promising ways to learn about the structure in liquids is to study the diffusion mechanisms in liquids. The mechanism of liquid diffusion is intricately related to the structure of liquids. The driving forces for mass transport can be derived mathematically from thermodynamics. However, present models and theories of liquid diffusion vary dramatically, especially with respect to the prediction of the temperature dependency of the diffusion coefficient.

It is of great importance to obtain highly accurate values of transport properties since only precise data will enable one to test the theoretical models and new theories and, in so doing, learn the underlying physical mechanisms.

2.3.1 Fick's Law

The first mathematical attempts to describe mass transport were the experiments in gases and liquids by Thomas Graham and Adolf E. Fick. From these, Fick's First Law was proposed to describe diffusion in a steady state. The linear Fick relation, which is analogous to Fourier's law for heat conduction and Ohm's Law for electrical conduction is represented by,[11]

$$J_T = -DA\frac{\partial C}{\partial x} \qquad (1)$$

where J_T represents the total flux, D is a constant characteristic of the pure material and is commonly known as the diffusion coefficient, A is the area crossed by the diffusion path, C is the concentration, and x is the distance.

For the non-steady, or time-dependent state of the diffusion process, Fick's Second Law is used. In the case of a constant or average diffusion coefficient in one dimension,[11]

$$\frac{\partial C}{\partial t} = D\frac{\partial^2 C}{\partial x^2} \qquad (2)$$

where t is the diffusion time. It is important to note that Fick's First and Second Laws describe mass transport as a result of a concentration gradient.

2.3.2 Conventional Description of Data – Quasicrystalline Model

In this model, the atoms in a liquid are assumed to be arranged in similar way to those in a solid. Thus, this model assumes a thermally activated diffusion mechanism where potential barriers must be overcome, as in solids. The relationship between temperature and the diffusion coefficient is therefore represented by the following equation,[5,7]

$$D = D_o \exp\left(-\frac{Q}{RT}\right) \qquad (3)$$

where Q is the activation enthalpy of diffusion, R is the gas constant, T is the temperature and D_o is a system constant. This model assumes that, similar to vacancies in solids, liquids must also contain voids in their microstructure. However, only the atoms nearest to the "hole", which is of critical dimensions, take part in the

diffusive displacement. The more remote atoms only undergo an oscillatory movement around a point and the fluid surrounding these atoms merely acts as an elastic medium. This model is also known as the Hole Theory of Liquids.

2.3.3 Stokes-Einstein Theory

In this, one of the oldest theories, the atomic diffusion coefficient, D, is expressed as the ratio of driving and friction forces.[12,13] It should be strictly applicable for relatively large diameter solutes, such as the macromolecules existing in solutions of proteins, diffusing in a solvent of low molecular weight.[11] To take into consideration the case when non-spherical shapes are present or when the solute and solvent molecules have similar diameters which can then cause a slip between the solute and solvent resulting in an increase in the diffusion coefficient, an additional factor can be introduced into the equation. In this theory, it is assumed that the diffusing species are non-reacting spherical particles of radius R moving through a continuous medium of viscosity η with a steady-state velocity. The temperature dependence of the diffusion coefficient is represented in the following equation,

$$D = \frac{kT}{6\pi R\eta} \qquad (4)$$

2.3.4 Nernst-Einstein Theory

This theory was originally derived for aqueous solutions but may also be applied to liquid metals.[14] When the mobility of the diffusing species is known

independently, a modification to equation (4) is made to calculate the diffusion coefficient, thus:

$$D = \frac{\mu RT}{N} = \mu kT \qquad (5)$$

where D is the diffusion coefficient, μ is the mobility of the diffusing species, k is the Boltzmann constant, and N is Avogadro's number.

2.3.5 Model of Critical Volume

In this free volume model, a critical volume, V*, is assumed to be necessary in the neighbourhood of a diffusing atom. Since the formation of such a free volume, V_f, is also assumed to be thermally activated, the diffusion coefficient is expressed by,[7]

$$D = A\sqrt{T}\exp\left(\frac{-bV^*}{V_f}\right) \qquad (6)$$

where V* is the critical volume associated with the diffusing atom, V_f is the free volume of the liquid, and A and b are constants of the system.

A modification of equation (6) has been made by Cohen and Turnbull. Their derivation is based on the idea that molecular transport occurs by the movement of molecules into voids, with a size greater than some critical value, formed by the redistribution of the free volume.[15]

While the molecules are normally confined to a cage bounded by their immediate neighbour and moving with a gas kinetic velocity, a fluctuation in density can cause a hole to open up in the cage. If this void is large enough, that is of a

critical volume, V*, then a neighbouring atom moves in. Such a displacement results in diffusion only if the atom jumps into the hole before the original atom returns to its position. Thus, the relationship between the diffusion coefficient and temperature is given by,[15]

$$D = ga^{*}u\exp\left(\frac{-\gamma V^{*}}{V_f}\right) \qquad (7)$$

where g is a geometric factor, a* approximately equals the molecular diameter (jump distance), u is the gas kinetic velocity, γ is a numerical factor introduced to correct for overlap of free volume (should lie between 0.5 and1), V* is the critical volume just large enough to permit another molecule to jump in after the displacement, and V_f is the average free volume (total free volume divided by the number of molecules).

This equation gives a moderately good representation of the data for both Van der Waals liquids and liquid metals at normal pressure.

2.3.6 Fluctuation Theory – Swalin 1959

In this theory, no critical volume is assumed to be necessary, which means that the particles move directly by fluctuation of the free volume. Swalin[16] postulated that diffusion results from the movement of atoms small and variable distances as a result of local density fluctuation. A given atom is surrounded by 10-12 other atoms and the probability of this atom being adjacent to a fluctuation of any magnitude is equal to one. The possible distance of a diffusion jump is variable and contrary to that in solids, is not a discrete value since a continuous distribution of

fluctuation sizes is to be expected. The atomic diffusion coefficient is then determined by the following equation,

$$D = AT^2 \qquad (8)$$

where A is a constant related to the interatomic potential.

Later, in a study of diffusion in liquid tin, Swalin[17] stated that in the case of solute diffusion, the probability and the magnitude of local density fluctuations in the vicinity of the solute atoms are the prime interest. Swalin also suggested that solutes with positive relative partial molal enthalpies are expected to have large and numerous density fluctuations close to the solute atoms and vice versa. The results of this study also suggested that the solutes which have large repulsive interactions with the solvent tend to diffuse faster than the solvent. However, solutes with large attractive interactions with the solvent tend to diffuse at the same rate as the solvent. Hence, this insinuates that the properties of the solvent itself govern the diffusion rate. Furthermore, Swalin proposed that in dilute solutions, the diffusion coefficient of a solute approaches that of the solvent if the solute has a zero or large negative relative partial molal enthalpy in the solvent.

The values of the diffusion coefficient derived with the above equation do not always fit the experimental data. This may be due to errors introduced into the experimental values, such as convection and the uncertainty of the atomic force parameters. Recent space experiments on self-diffusion of tin have given support to the T^2 dependency of the diffusion coefficient.[18]

2.3.7 Fluctuation Theory – Reynik 1969

In his study of diffusion in liquids, Reynik[19] suggested that for small fluctuations, the liquid diffusion model predicts a linear variation of the diffusion coefficient with temperature of the form,

$$D = -a + bT \qquad (9)$$

where

$$a = 1.72 \times 10^{24} Z x_0^4 K$$
$$b = 2.08 \times 10^{9} Z x_0^2 \quad ,$$

Z is the specified liquid state coordination number (first nearest neighbours), x_0 is the maximum diffusive displacement, and K is the force constant.

Reynik compared the results he obtained with mercury with those from Nachtrieb and Petit[20] for their study of self-diffusion in liquid mercury and found that they were in excellent agreement with the diffusive displacements calculated by of Nachtrieb.

Reynik stipulated that the assumption that during each vibration, the centre of oscillation of an atom moves a distance x_0, suggests that every atom and its first nearest neighbours are participating in irreversible, random-walk displacements on a time scale comparable to a vibrational period. Thus, as such, there is no "activation process" in the conventional sense.[19]

It is interesting to note that, approximately from the same basis as equation (8), equation (9) also has been derived. Reynik disputed the calculations of Swalin for equation (8) and proved that Swalin's prediction of a linear variation of D with T^2 was wrong, the corrected prediction being a linear variation of D with T.[21]

The model proved to be in excellent agreement with most of the terrestrial experimental data in liquid metals, alloys, organic alcohols, molten salts, and miscellaneous liquids. As a result, the calculated small diffusion displacements gave rise to serious doubts of the importance of atomic-sized holes in liquid diffusion processes.

2.3.8 Hardsphere Models

Using Enskog's theory[22], which assumes that an atom experiences a number of hard core binary collisions with its neighbours and that each successive collision is unrelated to the earlier one, the diffusion coefficient is calculated by the following equation,[22,23]

$$D_i^E = \frac{3}{8n\sigma_{is}^2 g_{is}(\sigma_{is})}\left(\frac{kT}{2\pi\mu}\right)^{\frac{1}{2}} \qquad (10)$$

where

$$\mu = \frac{m_i m_s}{m_i + m_s}, \qquad \sigma_{is} = \frac{1}{2}(\sigma_i + \sigma_s)$$

D^E_i is the binary collision diffusion coefficient of the solute "i" in the solvent "s" and "is" stands for the mixture of the binary solution, μ is the reduced mass, m is the mass, σ_i and σ_s are the hard-sphere diameters of solute and solvent atoms, respectively, k is the Boltzmann's constant, and $g_{is}(\sigma_{is})$ is the radial distribution function of unlike atoms at contact.

In order to take into account the successive collisions and many-body interactions, a correction factor must be used since Enskog's expression is insufficient in determining the properties of dense hard-sphere fluids.[24]

2.3.9 Molecular Dynamics

Another approach in studying diffusion is the use of molecular dynamics calculations. Essentially, to make molecular dynamics calculations, some force field between spheres with hard centres and soft shells must be chosen. In the simpler versions of the technique, a liquid metal is taken to be similar to a hard sphere fluid and that the transport in a hard sphere fluid is accurately described by the Enskog theory.

For such calculations, the atoms in the fluid are assumed to interact with each other by way of their inter-atomic potentials. A computer program is best able to perform these calculations. It calculates the trajectories by solving the equations of motion for a large number of atoms.[25] In this model, the temperature dependence of the diffusion coefficient is shown by,[24]

$$D = A^{1}T^{m} \qquad (11)$$

where m=1.7 – 2.3 and A^{1} is a system constant.

2.3.10 Summary

A number of models are proposed for the structure of liquids and the manner in which the rate of solute diffusion is controlled. Each of them exhibits a particular relationship between the diffusion coefficient and the temperature. They are summarized in Table 1.

Table 1 Theories/Models of Diffusion in Liquids

Diffusion Coefficient – Temperature relationship	Theory
$D = D_o \exp\left(-\frac{Q}{RT}\right)$	Conventional Description of Data
$D = \frac{kT}{6\pi R\eta}$	Stokes Einstein Theory
$D = A\sqrt{T}\exp\left(\frac{-bV^*}{V_f}\right)$	Model of Critical Volume
$D = AT^2$	Fluctuation Theory – Swalin 1959
$D = -a + bT$	Fluctuation Theory – Reynik 1969
$D_i^E = \frac{3}{8n\sigma_{is}^2 g_{is}(\sigma_{is})}\left(\frac{kT}{2\pi\mu}\right)^{\frac{1}{2}}$	Hardsphere Models
$D = A^1T^m$, $m = 1.7 - 2.3$	Molecular Dynamics

3 Experimental Procedures

3.1 Diffusion Couple Fabrication

For solid and liquid diffusion experiments, a diffusion couple is generally used. Usually, the two halves of the diffusion couple are prepared separately and then fit together. This method leads to various problems such as the presence of an oxide layer and of cavities or inclusions on the solid-solid interface. This interface between the two halves of the diffusion couple has to be sharp to be in accordance with the boundary conditions and should be similar to a planar grain boundary. These requirements have not been met in the past since in the solid-solid method, an oxide layer is impossible to eliminate and in the liquid-liquid method, such as the shear cell method, liquid mixing may degrade the sharpness of the interface. A novel method, called the cast coating technique, was developed by Zhu[26] and met all of the above requirements.

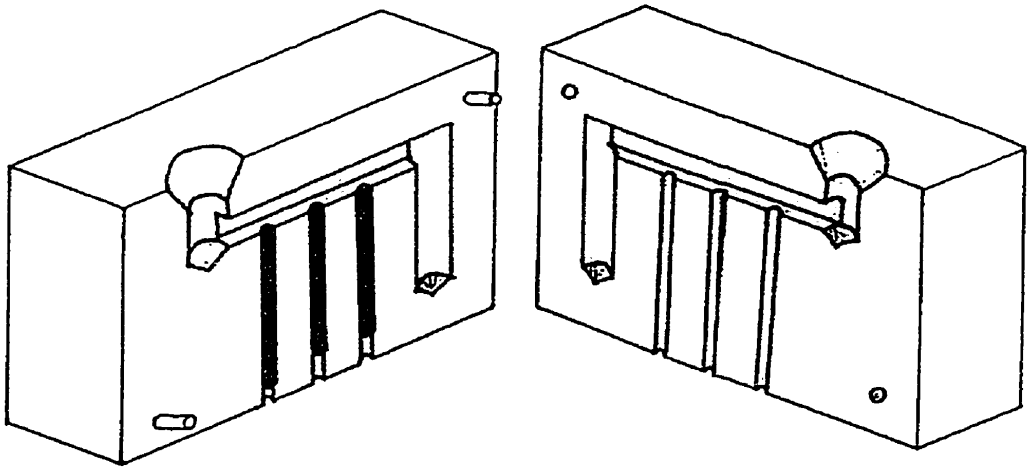

Figure 2 Cast Coating Mold

Semi-infinite diffusion couples were prepared for this study in which solvent rods were first produced by casting followed by swaging, cutting to length, and then

being placed in a chill mold such that their ends projected into a horizontal gallery, see Figure 2. The dilute alloy, typically solvent plus 1-2 wt% solute, was poured into the mold. In this study, three solvent metal systems were used, lead, antimony and indium, with solutes, silver, gold, indium, and antimony. Following casting, the finished specimen was cut from the alloy gallery by electro-discharge-machining (EDM). The careful selection of liquid alloy superheat and mold temperature permitted a clean planar interface to be obtained between the solvent rods and the solidified alloy.

The alloy systems were chosen to make best use of the temperature range available within the QUELD II furnace on MIR since, for safety reasons, the maximum temperature was 850°C. Referring to the phase diagrams[27] in Appendix III, it can be seen that the systems have homogeneous single phase liquids, a melting point close to that of the pure metal, a wide temperature range, and low melting points. In addition, antimony, metalloids and most common semi-conducting materials, are expected to have some covalent bonding in a liquid, which is just above the melting/liquidus temperature. Such bonding is expected to provide geometric clusters which could influence diffusion processes.

For this study, the long capillary method was chosen for the QUELD II samples.[28,29] It consisted of a long capillary containing the solvent to which a short alloy segment was attached when casting the sample using the device shown in Figure 2. The alloy layer in the upper part of the capillary tube must have a lower density than the melt in the lower part, if convection were to be avoided during manufacture. If this were not possible an inverted version of the mold is used with

the alloy segment in the base. Since the alloy segment usually has a concentration of only 1-2% of solute, its liquidus temperature will be close to that of the solvent. The long capillary method, developed by Zhu, was used since it provides high accuracy and safe and simple operation necessary for space experiments. It should be noted that to date, most space experiments studying diffusion in liquid metals have utilized this method. The shear cell has also been used but with limited success and no better accuracy.[3]

The diffusion couples were 1.5-3.0 mm in diameter and 40 mm in length. The length of the alloy segment was maintained at around 2.0 mm. The diffusion couple was placed in a graphite crucible, Figure 3, and sealed by a graphite cap. This graphite crucible was enclosed in a double-wall stainless steel sheath, Figure 4, by two laser welded end caps. A thermocouple would be inserted through the knurled end and make contact with the stainless steel plug segment, which the crucible was pressed by a second spring between the free-end of the crucible and the adjacent end-cap.

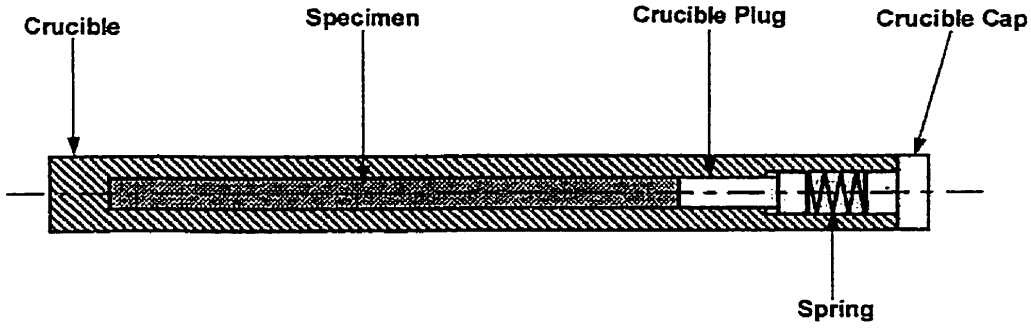

Figure 3 Schematic of the Graphite Crucible of a QUELD II Sample

Figure 3 is represented by the 81mm section in Figure 4, in which all the dimensions are in millimetres.

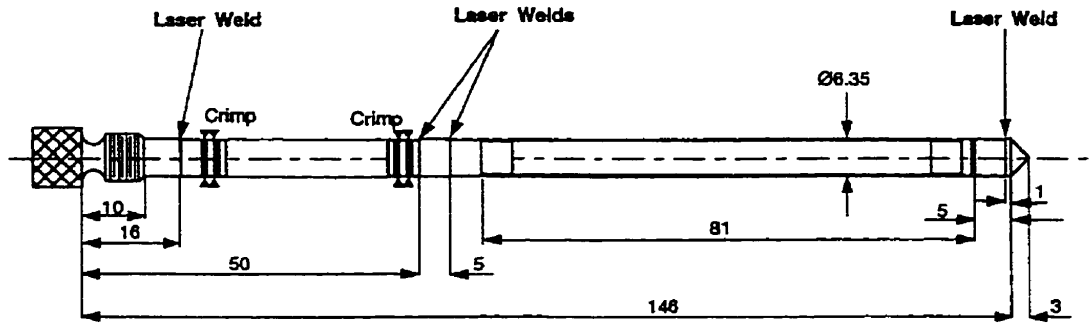

Figure 4 Schematic of the Longitudinal Cross-Section of a QUELD II Sample

3.2 Processing of the Diffusion Samples

In order to heat the specimen quickly to the diffusing temperature, the furnace was calibrated and pre-heated to a temperature above the anneal temperature. Upon the insertion of the specimen, the furnace was quenched to the desired diffusion temperature, see Figure 5.

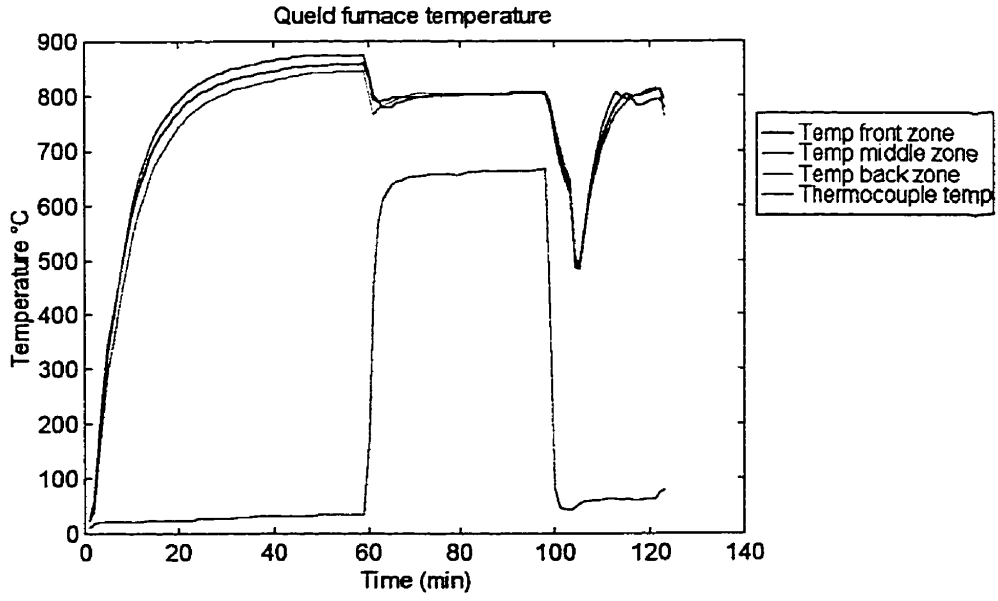

Figure 5 Temperature Profile of the QUELD II Space Unit for Sample 65

During the MIR programme, most of the diffusion couples were maintained at a fixed temperature and some were exposed to a temperature gradient for a given amount of time to permit the solute in the alloy part to diffuse into the solvent part of the diffusion couple. The diffusion-anneal period was selected to ensure that the semi-infinite diffusion boundary condition was not violated, i.e., no solute diffuses to the far end of the solvent section. Diffusion processing was performed for a series of temperatures and times, as shown in Table 2. The temperature was controlled to $\pm 1^{\circ}C$.

The method of quenching used in this study was evaluated and is described in detail in references 26 and 30. Following the diffusion anneal, spring-loaded aluminum quench blocks were brought into contact with the sample along that part of the sample surface covering the specimen in order to induce the radial removal of heat from the specimen (see Appendix I). This resulted in the rapid solidification of the specimen. Since the freezing front moves from the outer surface rapidly to the centre-line of the specimen, dendritic growth takes place, with any "solute pushing" being towards the centre-line of the specimen. However, since the scale of dendritic growth is much finer than that of the sample section used for determining the composition-distance plot of the diffusion couple specimen, local segregation does not influence the final composition determination. It is important to note that this method has worked effectively with alloy systems which contract on freezing (metal) and also those which expand (metalloids and semiconductors) when using graphite crucibles to contain the specimens.

Table 2 Processing Conditions for the Systems

Sample Number	System Solvent-**Solute**	MIM Mode	Diffusion-Anneal Temperature (°C)	Diffusion Time (hrs)
61	Pb-**Ag**	Isolated	400	1.10
62	Pb-**Ag**	Isolated	500	1.02
63	Pb-**Ag**	Isolated	600	0.93
64	Pb-**Ag**	Isolated	700	0.85
65	Pb-**Ag**	Isolated	800	0.67
67	Pb-**Au**	Isolated	600	0.83
82	Pb-**Sb**	Isolated	400	1.75
83	Pb-**Sb**	Isolated	550	1.30
84	Pb-**Sb**	Isolated	700	0.98
85	Pb-**Sb**	Isolated	800	0.83
238	In-**Sb**	Isolated	300	1.88
239	In-**Sb**	Isolated	400	1.70
240	In-**Sb**	Isolated	500	1.52
241	In-**Sb**	Isolated	600	1.33
242	In-**Sb**	Isolated	700	1.15
243	In-**Sb**	Isolated	800	0.97
245	Sb-**In**	Isolated	650	2.13
246	Sb-**In**	Isolated	700	1.75
247	Sb-**In**	Isolated	750	1.47
248	Sb-**In**	Isolated	800	1.17
401	Pb-**Au**	Forced[1]	400	0.33
402	Pb-**Ag**	Forced[1]	400	0.33
419	Pb-**Au**	Latched[2]	400	0.33
420	Pb-**Ag**	Latched[2]	400	0.33

[1]Forced oscillations: 0.1 Hz at 45° to sample axis

[2]Unconfirmed MIM Data

However, upon heating and cooling, flow problems arise near the melting point due to thermal expansion and volume change. In order to avoid surface tension

driven convection (Marangoni convection), any free surface between the diffusion couple and the crucible had to be eliminated. A spring-loaded piston was used to ensure no free-volume existed in contact with the specimen and in doing so, permitted the volume change, which occurred during the melting and freezing processes, as seen in Figure 3. Prior to the use of the quench block system for QUELD II on MIR, extensive modelling and physical testing took place at Queen's, on KC135 flights (parabolic flights), QUESTS I and II and QUELD I space flights. In this study, all the samples were processed using the QUELD II and MIM facilities on board the MIR space station, see Figure 6.

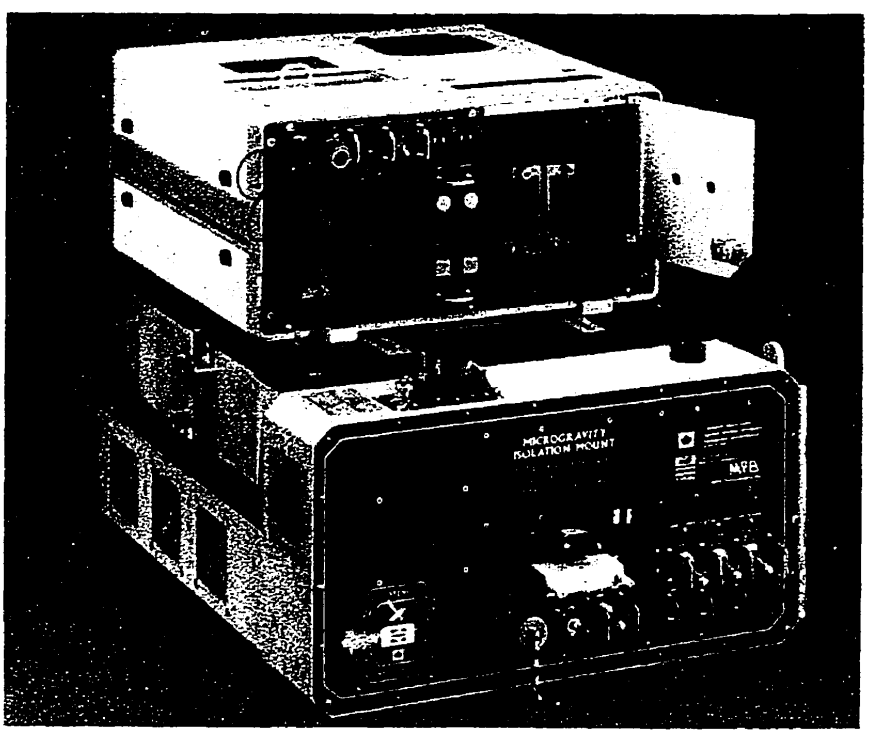

Figure 6 QUELD II Furnace on MIM (see Appendix I, II)

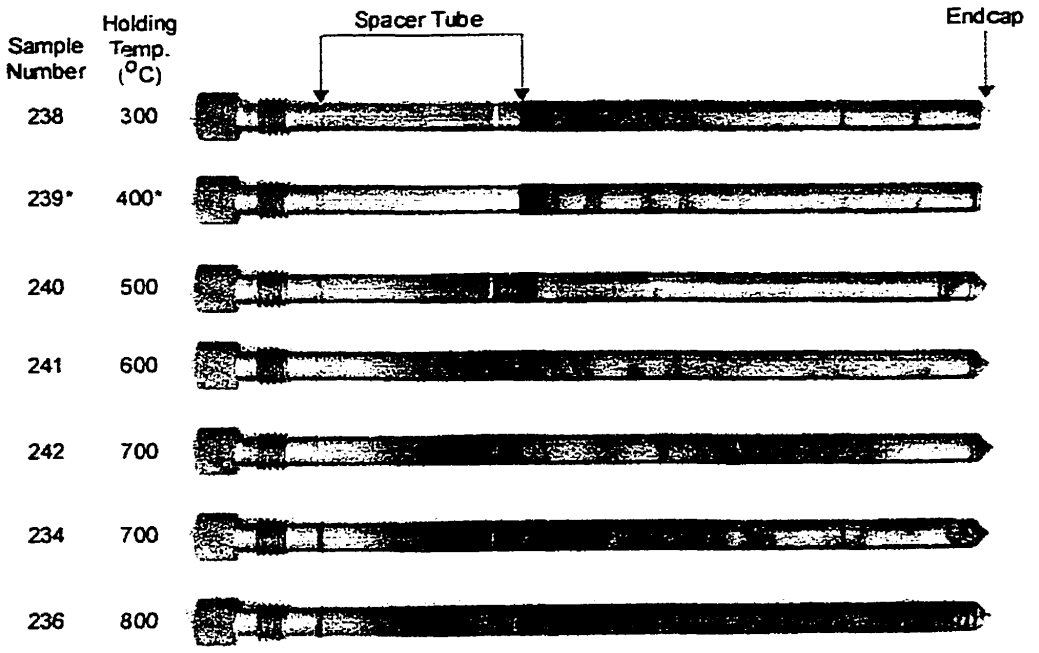

Figure 7 Colour Scheme Showing the Amount of Oxidation

3.3 Methodology for Analysis

3.3.1 Sample Preparation

Upon return to the ground, the space-processed samples were analyzed. During this process, a visual inspection of the outer stainless steel container was performed prior to opening the container. The amount of oxidation present on the spacer tube and the end cap, represented by a colour change, may be related to the processing temperature, as shown in Figure 7.[31] This initial inspection permitted the verification of the processing temperature. As can be seen from Figure 7, one sample was not processed due to technical difficulties encountered on the space station. A

total of two samples were unprocessed. The chemical analysis proved that this initial assumption was correct for both cases, as can be seen in Appendix IV.

After opening the three levels of containment, another visual inspection was performed. This was done to take note of any defects or anomalies that would affect the results, as shown in Figure 8. As can be seen from this photograph, there was a very slight variation in length and diameter, which was representative of the systems that were studied in this work. These observations were found to have negligible effect on the overall calculations of the diffusion coefficients.

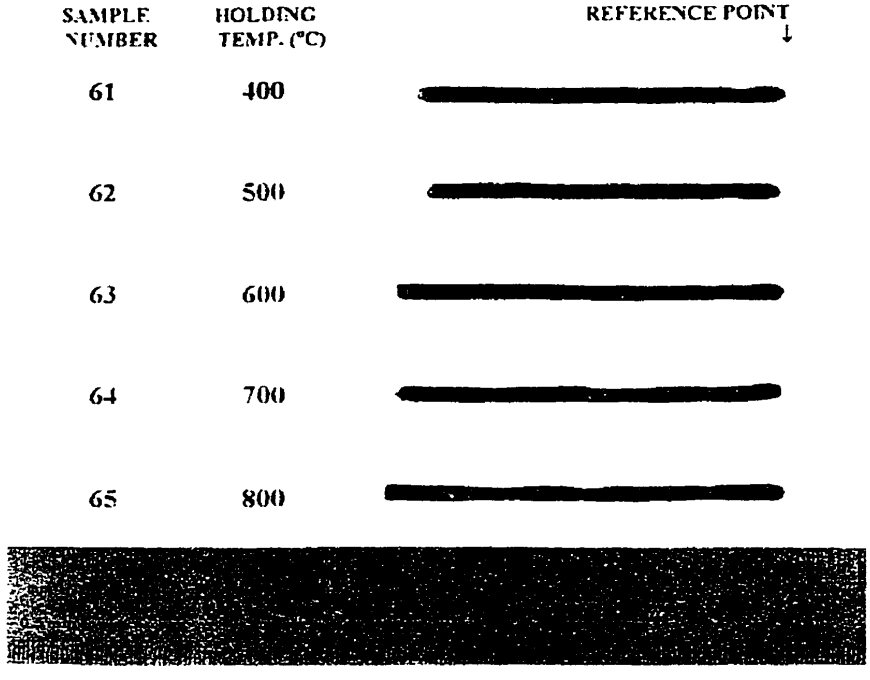

Figure 8 Picture of Pb-Ag Samples Processed Over a Temperature Range

The diffusion couples were cleaned using acetone and their length was measured. Each sample was sectioned by cutting perpendicular to the diffusion direction; the first section being 1.5 mm in length and the others, 2.0 mm in length.

The first section needed to be of a smaller length due to the higher concentration of the solute present and, in doing so, avoided subsequent dilutions that would introduce errors in the chemical analysis. Two different types of apparatus were used to section the samples, depending on whether the sample was ductile or brittle. In the case of a ductile solvent, i.e., lead and indium, a customized apparatus was used which consisted of a micrometer and a positioning device for the blade. This method was proven to be accurate and was extensively used in work by Zhu.[26]

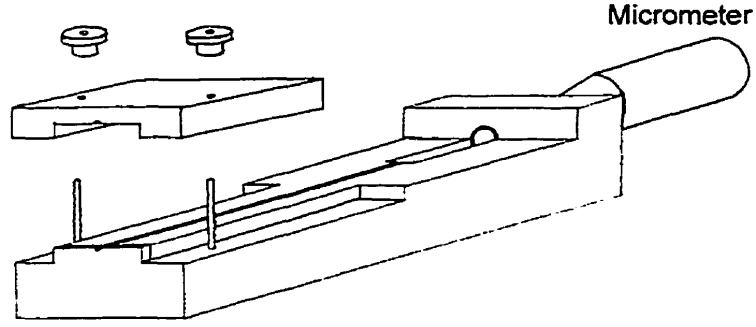

Figure 9 Sectioning Apparatus for Ductile Diffusion Samples

However, when the solvent was antimony, the sample was very brittle. After a few trials with dummy samples, it became apparent that this customized method was not satisfactory since it failed to provide a sharp and clean cut. The antimony-rich dummy sample would fracture into several pieces. Hence it was necessary to develop an alternative effective sectioning method for the brittle antimony-rich samples. As a result, a small specimen jig was made which could be used with the electro-discharge machine (EDM). This was found to be very effective permitting cutting with an accuracy of ±0.013 mm, as confirmed by measurement. All the samples which consisted of antimony as the solvent were sectioned with the EDM method. Proper calibration of this method was performed and several practice

samples were sectioned prior to the space samples. Since the EDM method uses a fine copper wire to discharge the electrical current and consumes part of each section, it was necessary to ensure that this length was included in the calculations for the distance to the reference point. Each section was then weighed to 0.1 mg accuracy using a digital balance.

3.3.2 Atomic Absorption Spectrophotometer

As mentioned earlier in section 3.2, there may be segregation problems with the spot analysis methods such as the electron micro-probe technique. In view of this, the atomic absorption spectrophotometry technique was used to measure the solute concentration of each section.

Atomic absorption spectrophotometry (AAS) involves the study of absorption of radiant energy by neutral atoms in the gaseous ground state. In atomic absorption analysis, the sample solution is drawn into the instrument, vaporized as tiny droplets which are then decomposed into their elemental states in a flame which burns under specific conditions. Thus, within the flame a gaseous solution or plasma containing a significant concentration of atom species is produced. This is the method of choice for the determination of a large number of metals, especially at trace levels. More than 60 elements can be determined by AAS and hence it is widely used in metallurgy for the analysis of the minor constituents of alloys.[32]

3.3.2.1 Interferences

AAS is a very specific technique with few interferences. The ones that do exist fall into six categories: chemical, ionization, matrix, emission, spectral, and

background interference. Emission interference relates to atomic emission; this does not apply in this work since throughout the analysis, atomic absorption was used.

Chemical interference is the most common interference in atomic absorption. It occurs when a thermally stable compound is found in the sample to be analyzed and is not completely decomposed by the flame. This results in a reduced number of atoms in the flame capable of absorbing the light. Due to the simplicity of the systems to be analyzed, i.e., only two component systems, this kind of interference did not occur.

Ionization interference consists of the removal of an electron from the atom, creating an ion and is caused by the high flame temperature. As a result, atomic absorption is reduced due to a depletion of the number of ground state atoms. Since only an air-acetylene flame, with a temperature of about 2300°C, was used in this study, compared to a nitrous-oxide-acetylene flame with a temperature of about 2900°C, the possibility of ionization interference is highly unlikely. Also, all the elements of interest have high ionization potentials.

When any physical characteristic, such as viscosity, of the sample and the standard differ considerably, matrix interference occurs and can cause either a suppression or enhancement of the absorbance. Since nitric acid and/or hydrochloric acid was used, several runs were made with different concentrations of acid to verify the extent of the acid concentration affecting the absorbance. As the concentration of the acid was increased, the sample viscosity increased, slowing down the introduction rate and reducing the sample absorbance. Since the concentration of the acid changed the viscosity of the solution, the amount of acid was kept to a minimum. The same

concentration of acid was added to the standards, using a calibrated volumetric pipette, and they were also heated for the same time as the corresponding samples. In doing so, the matrix of the sample and the standards were matched as closely as possible and hence, matrix interference was kept at a negligible level.

Spectral interference can happen when an other element, which is not being determined, is present in the sample and has an absorbing wavelength that falls within the bandwidth of the absorption line of the element of interest. This is most common when using multi-element lamps, however, only single-element lamps were used in this work. In the event of spectral interference, the absorbance becomes erroneously high but may be easily remedied.

Finally, background interference is caused as a result of light scattering by particles in the flame and molecular absorption of light from the lamp by molecules in the flame. The use of a background correction factor is the most common way to compensate for background absorption. However, background correction is not recommended at high wavelengths and can even be detrimental to the analysis. The only element that needed background correction was antimony since it has a small wavelength. Thus, background interference was kept at a negligible amount during the analysis procedures.

3.3.2.2 Possible Sources of Error

Even though the AAS technique for chemical analysis is relatively simple, errors can be easily introduced if proper preparation of the samples and the instrument are not carefully performed. In order to get familiarized with AAS technique, it was necessary to spend two weeks with the Analytical Services Unit and

to perform a wide range of analysis using three different AAS instruments. To obtain valid results, it is imperative to carry out adequate sample preparation and this starts even at the cleaning of the volumetric flasks. Since the prior usage of the flasks was unknown and in most cases, heat was necessary to dissolve the samples, some residue might have been attached to the glass. Such residue might not be seen with the naked eye and might not be easily removed just with a simple rinsing. To minimize this accumulation of residue, all the flasks and their stoppers were immersed in a 10% nitric acid bath for a period of at least 36-48 hours. The flasks were then rinsed with deionized distilled water and, rinsed again with approximately 20% nitric acid and finally rinsed with deionized distilled water. The volumetric flask size varied between 25-100 ml and were Class A flasks that had been checked to ±0.01% accuracy. The range of volume sizes was necessary to maximize the absorbance indication on the AAS instrument and to avoid subsequent dilutions of a solution with a relatively higher concentration.

Before conducting an AAS analysis, optimization of the AAS instrument was carried-out. For example, the length of the nebulizer capillary, which is the small plastic tube through which the solution is aspirated, has to be maximized to indicate the most absorbance. Also, the nebulizer flow needs to be maximized, as well as the position of the burner head, which can be moved along the three axes.

The sensitivity of the AAS technique depends on the element of interest. For most elements, it is about 0.01 ppm and the accuracy of measurement is generally about 1-2%. This corresponds to an elemental sensitivity of 0.002 in weight percent and the accuracy ranges between 0.004% to 0.2% in the composition analysis of the

alloy specimen.[26] Error bars on the diffusion coefficients, plotted in the results section, were not included as the work by Frohberg[5] reported negligible uncertainty when samples were processed under microgravity conditions.

To summarize, the factors affecting accuracy for a high-precision analysis are: the analytical balance used, the volumetric pipetting, volumetric flasks, cleanliness of the equipment, purity of the acids used, control of the AAS interferences, standard solution preparation, optimization, and calibration of the AAS instrument. All of these factors were thoroughly investigated in order to maintain them at minimum values.

3.3.2.3 Sample Analysis

In order to use AAS, the resulting sections must be dissolved into aqueous solutions. Depending on the element, nitric acid and/or hydrochloric acid was used to dissolve the samples on low heat setting of the hot plate, i.e., 50-70°C. The sections of the Pb-Ag, In-Sb, and Pb-Sb systems were dissolved with nitric acid, while the ones of the Sb-In system required hydrochloric acid. Both nitric acid and hydrochloric acid was necessary to dissolve the sections of the Pb-Au system. The sections of the Pb-Au system required special attention since a lead chloride precipitate would form, if proper precautions were not taken. After dissolution and as soon as the solution was at room temperature, it was essential to proceed with the AAS analysis immediately, if the precipitate were to be avoided.

Each section was appropriately identified and dissolved to form a sample solution in a volumetric flask. The AAS technique was then used to determine the concentration of each section. The atomic absorption spectrophotometer has a built-

in calibration feature that calculates directly the concentration of the element of interest in the solution. However, this feature was not used in this study since it does not provide the user with an adequate representation of the raw data. Hence standard solutions were made and kept in the linear absorbance range and the calibration curve was manually calculated using a spreadsheet software. This will be discussed in detail in the results section. All the systems, except when determining the concentration of antimony, were analyzed with a Perkin-Elmer AAS instrument, Model 2380, located in the Materials and Metallurgical Engineering Department. The analysis of antimony required the background correction feature on the spectrophotometer, thus, the analysis was performed on a Varian AAS instrument located in the Analytical Services Unit of Queen's University.

4 Results and Discussion

4.1 Concentration Profiles

The usefulness of absorption in spectroscopy as a quantitative analytical method comes from the fact that the absorbance, A, can be related to the concentration of the analyte in a relationship known as Beer's law,

$$A = \varepsilon \cdot b \cdot C \qquad (12)$$

where C is the concentration of analyte, b the lightpath and ε a quantity know as the molar absorptivity. For a given irradiation wavelength, ε is a constant characteristic of a particular species. Therefore, a plot of A versus C should give a straight line for a given species at a fixed irradiation wavelength.[33]

Hence, the absorbance of the standard solutions were plotted against their concentrations, Figure 10, instead of using the built-in calibration feature on the AAS, as mentioned in the previous section. In doing so, the quality of the standard solutions and the accuracy of the analysis can be verified. As can be seen in Figure 10 the slope is calculated using linear regression and the 95% confidence limit and the prediction interval are also plotted. The narrow width of the prediction interval emphasizes the reproducibility of AAS technique while the 95% confidence limit reflects the accuracy of the AAS. The slope is used to calculate the concentration of each section of the specimen.

The concentration distribution profile was generated by plotting the composition of successive points along the specimen axis. Each point on the composition-distance curve corresponds to a cross section of the sample, Figure 11.

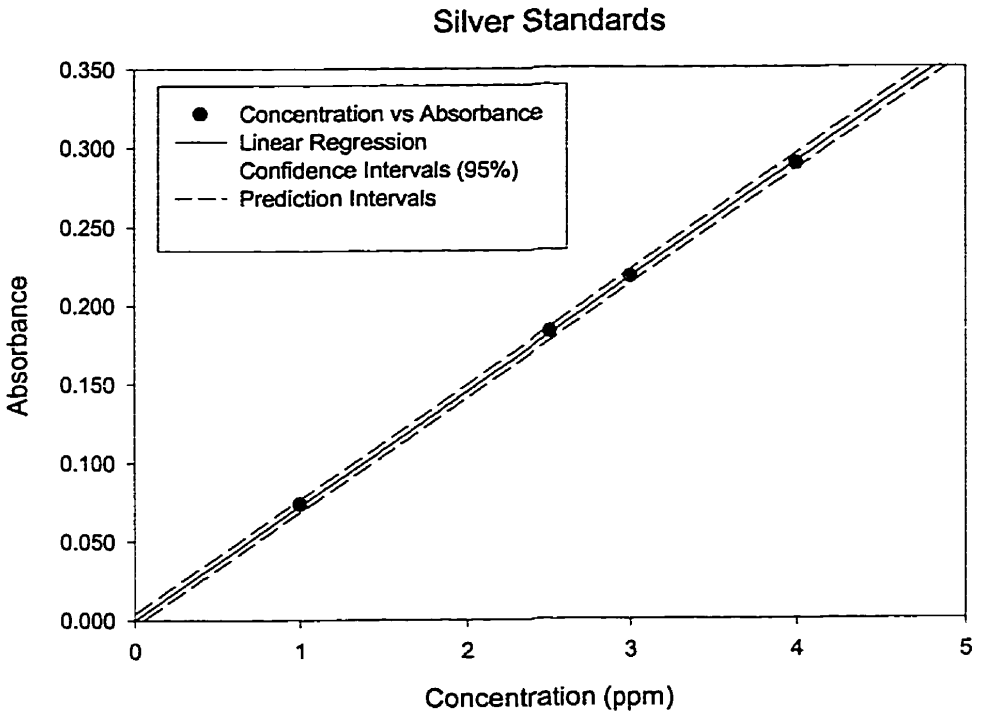

Figure 10 Calibration Curve for Silver

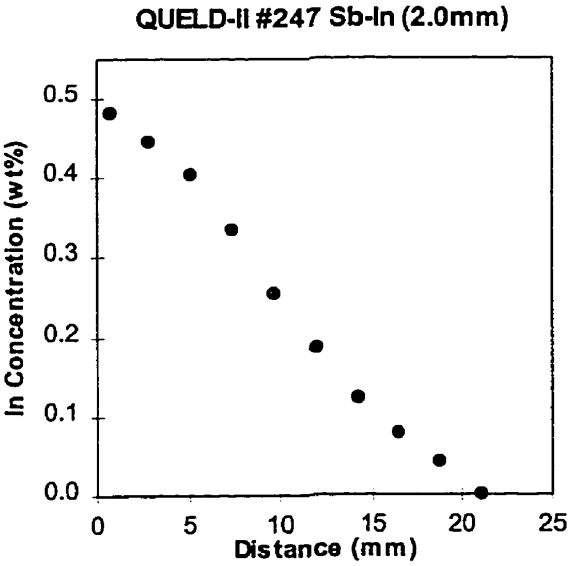

Figure 11 Concentration Profile of Indium Diffusing into Antimony

The results are presented in ppm and are then coverted to weight percent by,

$$wt\% = \frac{(ppm)(vol.[ml])(10^{-4})}{weight[gram]} \qquad (13)$$

For the concentration profiles of all the samples, refer to Appendix IV.

4.2 Determination of the Diffusion Coefficient

The long capillary specimen assembly technique combined with the semi-infinite diffusion couple was selected as a suitable experimental method, and so Fick's Second Law can be applied, namely:

$$\frac{\partial C}{\partial t} = D\frac{\partial^2 C}{\partial x^2} \qquad (14)$$

where C is the concentration at distance x, D is the diffusion coefficient, and t is the diffusion time.

For dilute solutions, D is constant and for a semi-infinite diffusion couple, with the following initial and boundary conditions:

For $t = 0$ and when $0 < x < d$, $C = C_o$ and when $x > d$, $C = 0$

For $t = t$ and when $x =$ infinite, $C = 0$

equation (14) has the following solution:

$$C(x,t) = \frac{C_o d}{\sqrt{\pi Dt}} \exp\left(-\frac{x^2}{4Dt}\right) \qquad (15)$$

where C_o and d are the initial concentration and length of the alloy part of the diffusion couple, respectively. "d" has to be very small compared to the whole diffusion length.

Taking the natural logarithm of equation (15) gives,

$$\ln C = \ln \frac{C_o d}{\sqrt{\pi Dt}} - \frac{x^2}{4Dt} \qquad (16)$$

By plotting lnC as a function of distance squared, a straight line is obtained, where

$$\text{slope} = \frac{-1}{4Dt}$$
$$\therefore D = \frac{-1}{(\text{slope})(4t)} \qquad (17)$$

It is important to note that the diffusion coefficient can be calculated in this manner if the condition of a constant diffusion coefficient can be achieved with dilute solution alloys. A typical plot representative of equations (16) and (17) can be found in Figure 12 while the plots of the remaining diffusion couples can be found in Appendix IV.

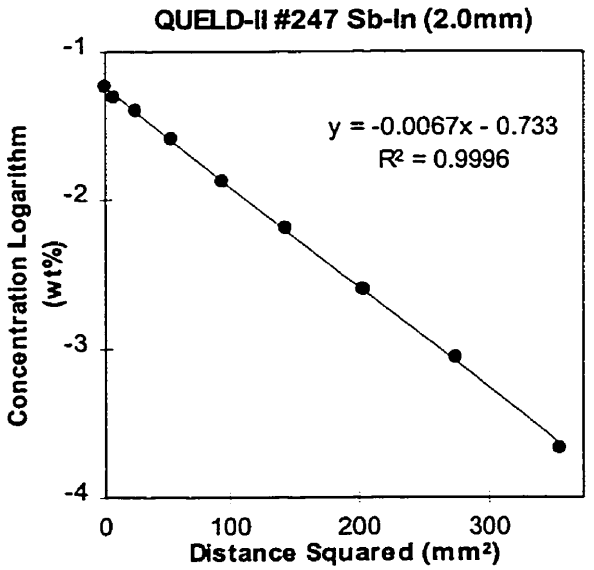

Figure 12 Regression Analysis of the Concentration Profile

The R^2 parameter is a measure of the "goodness of fit" of the regression, i.e., whether the calculated model fits the experimental data. To be considered an

adequate fit of the data, the R^2 value should be in excess of 0.95. All the samples had a value greater than 0.95 except the samples that were rejected before analysis for other reasons and so were not processed (Appendix IV).

4.3 Results of the Diffusion Coefficients

One hundred and fifty diffusion couple samples were prepared at Queen's University for the liquid metal diffusion studies of the MIR/MIM/QUELD II mission, twenty four of which were analyzed in this work. These samples were designed for liquid diffusion studies in ten alloy systems of varying solvent-type, solute addition, sample size (1.5, 2.0, and 3.0 mm in diameter) and experimental conditions, i.e., diffusion-anneal temperature, and MIM condition (isolating, latched, or forcing). This work is still in progress but some of the early experimental results are reported here.

4.3.1 Lead-Gold System

Figure 13 depicts the results obtained earlier with the STS flights 47 and 52 respectively, of QUESTS I and QUELD I and the equivalent 1g values. These were obtained for long capillary (semi-infinite) 1 mm diameter samples in which a 2 mm section of Pb-1wt% Au alloy was attached to a 38 mm pure lead filament. The Pb and Au were of at least 99.999wt% purity. It is seen that the microgravity results lie below those corresponding to terrestrial measurements.[30] For comparison, the variation of D with temperature for Pb-Au, calculated using the hard sphere model (HS) of liquid metals[34], is also given. It is seen that the latter quite closely represents the 1g behaviour but is significantly higher than the microgravity-derived data.

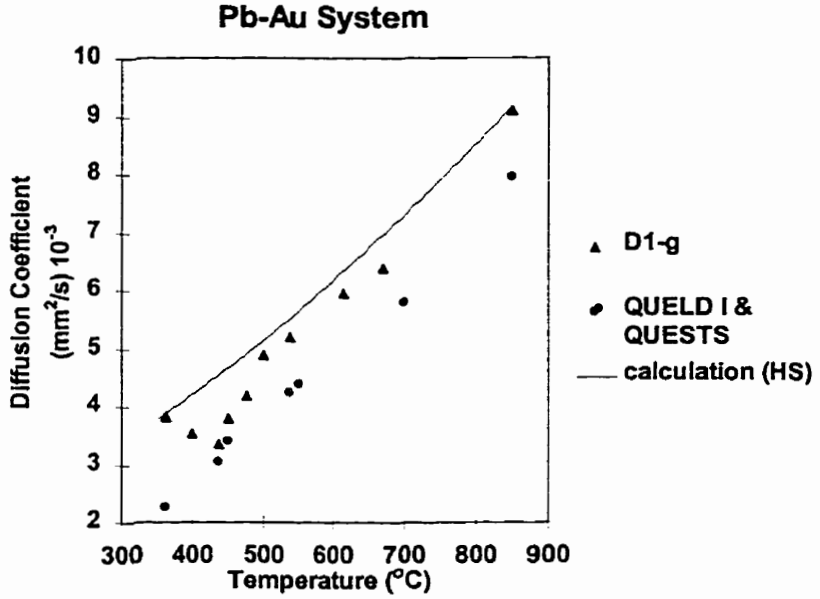

Figure 13 Diffusion Coefficients of Gold in Lead
Space and Ground-based Experiment Results

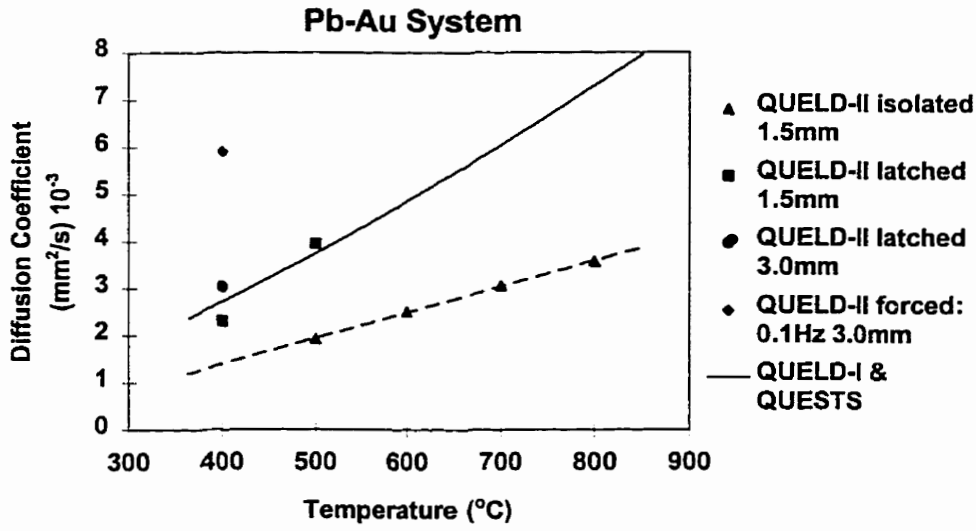

Figure 14 Diffusion Coefficients of Gold in Lead (3 MIM Modes)

Figure 14 shows some of the early data obtained from the MIR/MIM/QUELD mission. Here the earlier QUEST I/QUELD I data of Figure 13 are represented by the solid line in Figure 14. Significantly below this lie the data points obtained with MIM in isolating mode but using specimens of 1.5mm diameter.

The results from the g-jitter isolation experiments are very interesting. The diffusion coefficients obtained are lower than those from latched experiments, as expected. However, the difference is significant, since, in comparison with QUESTS I/QUELD I results, the diffusion coefficients from QUELD II g-jitter isolation experiments are about 50% lower. Of particular note is the fact that while the curves for QUELD I and QUESTS I data are concave upwards, that for g-jitter isolation is essentially a straight line, i.e., $D \propto T$, over the range of temperature studied.

It is noted that the D values produced with MIM in latched mode, correspond closely with the equivalent values derived from earlier QUESTS I/QUELD I experiments on the Shuttle. This suggests that, as far as gathering high-fidelity liquid diffusion data using small diameter specimens is concerned, the reduced gravity environment of the MIR is no "worse" than that of the Shuttle. Also, it is seen that the diffusion coefficient obtained with a larger specimen diameter (3 mm), and with MIM in latched mode, is somewhat larger than that of the equivalent specimen of smaller diameter (1 mm) used earlier with QUESTS I/QUELD I. This is to be expected since g-jitter is likely to be able to create more convective transport in larger diameter diffusion couples.

Also shown in Figure 14 is the effect of using MIM in forcing mode to superimpose a forced oscillation of 0.1 Hz upon the MIM isolating condition for a 3 mm sample. The forced oscillation resulted in a mean flotor acceleration of 4 milli-g at 45° to the long axis of the diffusion couple. The resulting D value is twice as large as that of a 1.5 mm diameter MIM-latched sample, a reflection of the increased mass transport induced by the forced oscillation.

4.3.2 Lead-Silver System

As with the Pb-Au system described above, here a 2 mm section of Pb-1wt% Ag alloy was attached to a 38 mm pure lead filament. Again, metals of 99.999% purity were used. The diffusion coefficient data obtained with the Pb-Ag diffusion couples are shown in Figure 15. The data were obtained with the MIM in the isolated mode. It is seen that these data points may be fitted closely to a $D \propto T$ (linear) relationship. For comparison, the full curve shown in Figure 15 is that for $D \propto T^2$, based on the D value for 400°C.

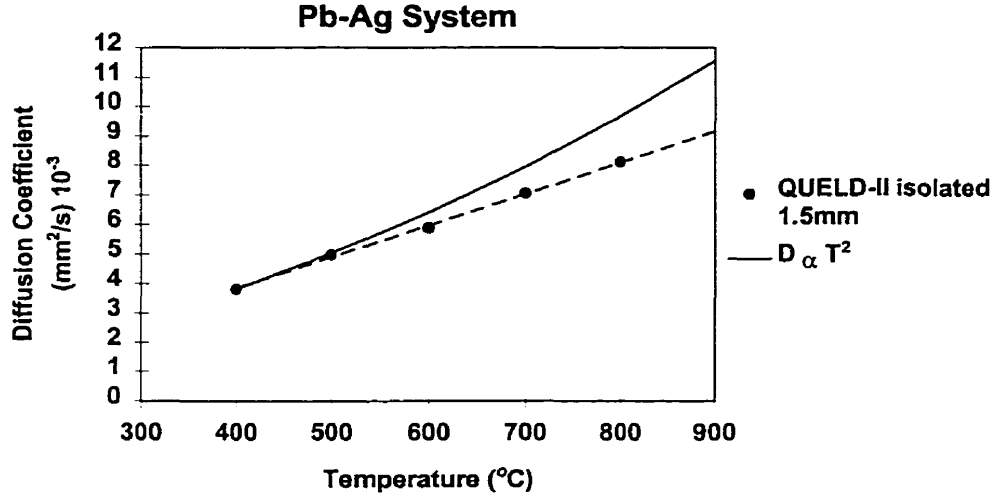

Figure 15 Diffusion Coefficients of Silver in Lead

4.3.3 Antimony-Indium System

Using Sb/Sb-1wt% In diffusion couples prepared as for Pb-Au diffusion couple, limited data for the diffusion of indium in liquid antimony, measured with MIM in the isolated mode, were obtained and are shown in Figure 16. A near-linear relationship of D with T is suggested.

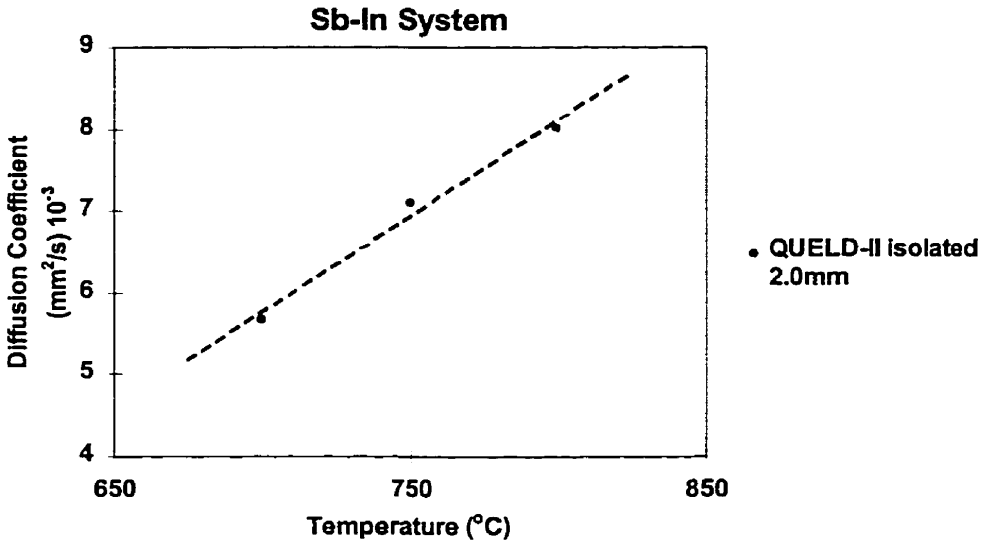

Figure 16 Diffusion Coefficients of Indium in Antimony

4.3.4 Indium-Antimony System

Similar data to that of Sb-In are shown for the diffusion of antimony in liquid indium, Figure 17, again using a 1wt% alloy diffusion couple. A near-linear relationship of D with T is again suggested.

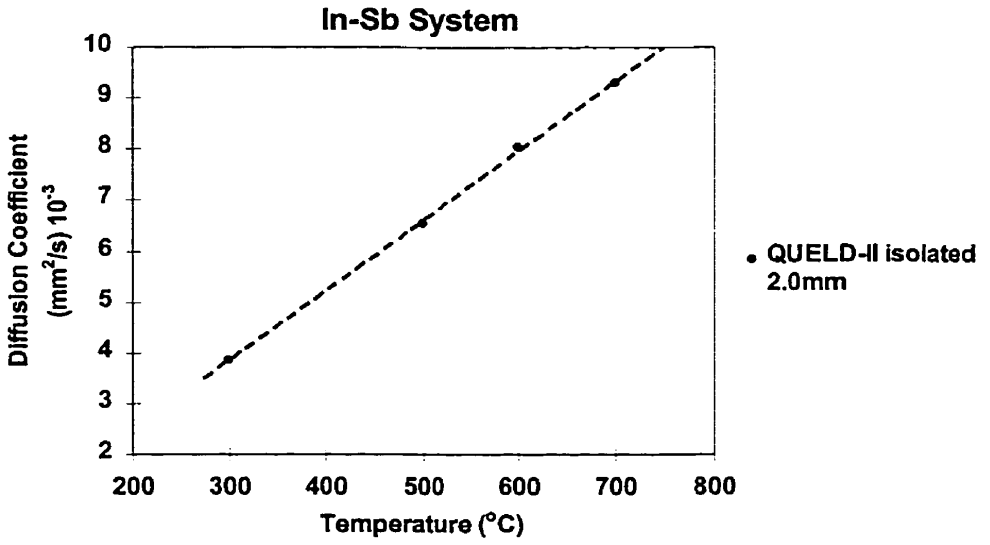

Figure 17 Diffusion Coefficients of Antimony in Indium

As can be seen from Figure 17, there is no data point for the sample processed at 400°C, diffusion couple #239. This is due to the visual inspection of the outer stainless steel spacer tube shown in Figure 6, which suggested, due to the absence of an oxidation color change, that it was highly unlikely that the sample was processed at the specified temperature. The concentration profile and the regression analysis of this unprocessed sample can be found in Appendix IV.

4.3.5 Lead-Antimony System

Again, similar data to In-Sb were observed. The diffusion couples were prepared as per the Pb-Au diffusion couples using a 1 wt% alloy and also measured with MIM in the isolated mode. A near-linear relationship of D with T is once more suggested in Figure 18.

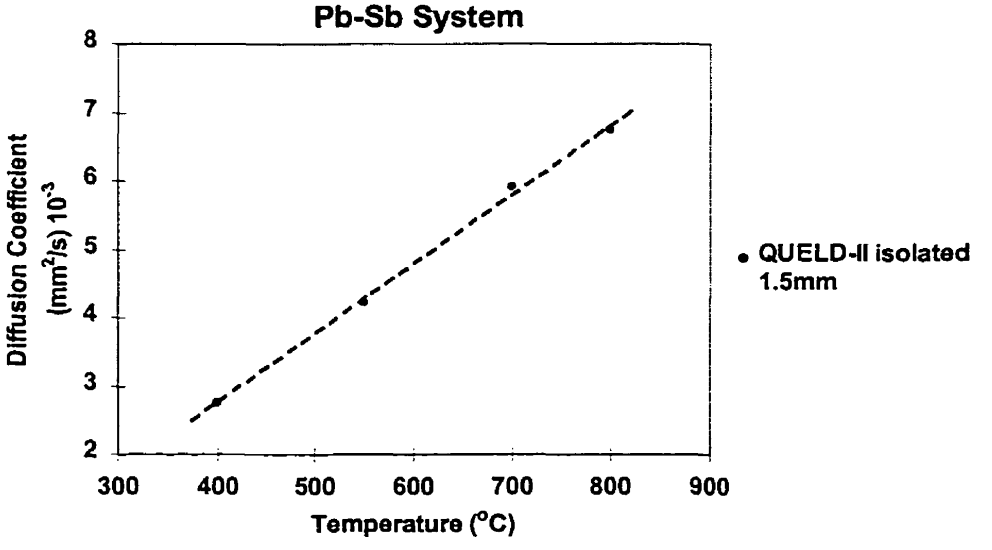

Figure 18 Diffusion Coefficients of Antimony in Lead

4.3.6 Lead-Solute Systems

Some superficial trends may be seen in the data presented in Figure 14, Figure 15, and Figure 18. A comparison can be made as the solvent for all three systems is

lead. It would appear that as the mass of the diffusing ion increases, so the increase in the diffusion rate induced by temperature increase decreases. Also, it is interesting to note that the diffusivity at the melting point of the alloy varies inversely but not linearly as the atomic mass of the solute, see Table 3.

Table 3 Superficial Correlations of the Lead Solvent Systems

Solute (Valence)	Slope of Diffusion Coefficient vs Temperature	Atomic Weight	Melting Temperature of the Alloy (K)	Diffusion Coefficient at Melting Temperature of the Alloy (mm^2/s) 10^{-3}
Silver (IB)	0.0107	107.87	583.15	5.80
Antimony (VA)	0.0102	121.75	583.15	4.60
Gold (IB)	0.0055	196.97	593.15	2.45

4.4 Discussion

There have been a number of models proposed for the structure of liquid metals and the manner in which this controls the rate of solute diffusion. Each model predicts a particular relationship of the diffusion coefficients with temperature. These are summarized in Table 1. However, in order to comment on the validity of any one model, it is necessary to have high quality data for selected alloy systems. As noted earlier, stray convection has confounded terrestrial experiments and in doing so, degraded the quality of the data obtained. The use of microgravity research facilities has permitted an increased data quality to be obtained in liquid diffusion experiments.

Figure 13 shows that the effects of convection in terrestrial experiments on Pb-Au alloys are significant, the diffusion coefficient falling markedly when similar experiments are performed on spacecraft. However, the experimental examination of the physical effects of the time-dependent variations in the gravity level aboard a spacecraft has only been possible with the relatively recent development of the MIM-type disturbance isolating system.

While the experimental procedures adopted and reported here may not reveal the truly intrinsic value of the diffusion coefficient for a particular alloy system, they give values which are much closer to this ideal value and so should more easily permit a detailed correlation of experiment with theory. It is anticipated that such a correlation may be possible when all the results of the present study are available, probably early 2000. However, some features of the present results should be highlighted.

The influence of low frequency (0.1 Hz) oscillation at 45° to the specimen axis was found to produce an observable increase in the measured value of the diffusion coefficient for the Pb-Au alloy, as had been anticipated. Since a detailed analysis of the effects of forced vibration on liquid diffusion couples of the dimensions used in this series of experiments was not available when planning the experiments, a forced oscillation of 0.1 Hz, but with a high harmonic content approaching that of a square wave (i.e., a square wave form), was requested for the processing of some of the diffusion samples.

Therefore, this forced oscillation of 0.1 Hz would provide a fundamental oscillation mode of maximum amplitude of 4 mg and at 0.1 Hz, plus a range of harmonics at various frequencies and amplitudes, see Appendix II. This was chosen on the basis that, since there was no clear description of the atomic movements involved in liquid diffusion, a variety of forcing modes might all contribute to the solute redistribution process. This would be in addition to the bulk convective transport induced in the sample by the low frequency components of the forcing oscillation. As is seen in Figure 14, the value of the diffusion coefficient was about double that of the Pb-Au in the latched mode.

The most successful and systematic study of self and inter-diffusion in liquid metals in the 1980's is Frohberg's work in the Sn system. One conclusion obtained was that the temperature dependence of the diffusion coefficient obeys the predictions of the fluctuation theory more closely than an Arrhenius-type relationship for both self and inter-diffusion in liquid Sn-In.[3]

When considering the marked reduction in diffusion coefficient in the absence of significant g-jitter and the fact that it was found that $D \propto T$ for all the alloy sytems examined, attention is directed to Figure 19.[35]

Here the work by Frohberg *et al.* demonstrated how the diffusion coefficient varied with temperature for various types of experimental environments. In the 1g case, the variation was a power law relationship which may be approximated by an exponential relationship while in the case of the microgravity experimental results, with g-jitter present, it has best represented by a $D \propto T^2$ relationship.

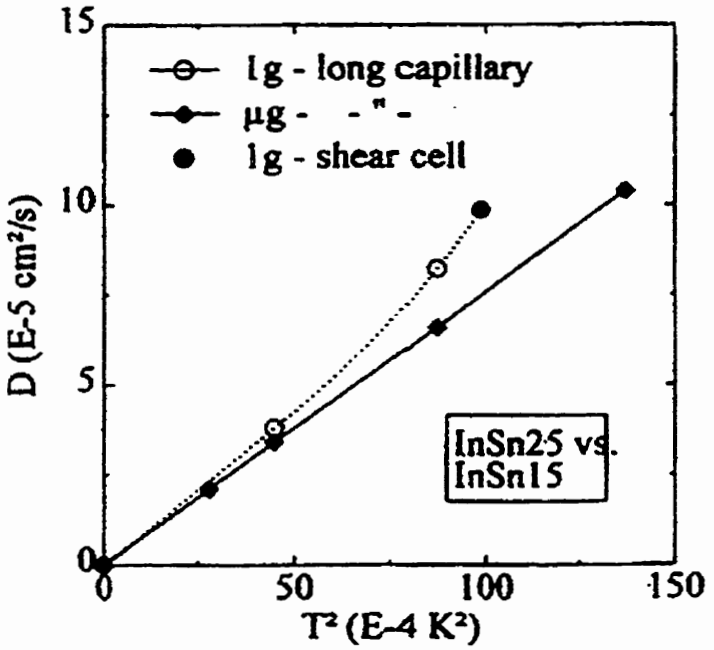

Figure 19 Diffusion Coefficients in the In-Sb System[35]

As it can be seen in Figure 19, experiments with the long capillary technique were made in microgravity and on the ground, 1g, while the shear cell technique was used for the experiments on the ground only. It becomes apparent that the diffusion coefficient is independent of the measurement technique.

However, as the contribution to mass transport by g-jitter is reduced by using the MIM in the isolating mode, the diffusion coefficient and temperature relationship becomes linear, as seen in the results section of this thesis.

Returning to the $D \propto T$ behaviour reported here, it should be noted that while Frohberg *et al*[35] have reported a $D \propto T^2$ relationship for experiments conducted without the benefit of a MIM, $D \propto T$ is commonly observed to describe both fluidity ($\equiv$ reciprocal viscosity) and diffusion in non-electrolyte liquids, if care is taken to suppress buoyancy-driven liquid flows. This view has been championed by a number of researchers, particularly Hildebrand.[36] This is shown, for example, in Figure 20. In particular the measured diffusion rates for various species in CCl_4 and C_6H_6 is closely linear with temperature over the temperature range tested. The corruption of data by buoyancy effects was rendered insignificant by measuring the diffusion coefficient using Fick's First Law, i.e., the flow of the chosen species through a membrane is given by

$$\text{Flux} = D\frac{\partial C}{\partial x} \qquad (18)$$

where C is the concentration and x is the distance.

In these experiments, the membrane between the species source and the large solvent-vessel beneath it consisted of a 9 mm thick slab of 2962 lengths of fine bore stainless steel hypodermic tubing in a parallel array and imbedded in solder. The small diameter of the hypodermic tubing effectively dampened-out any buoyancy contributions to the observed value of the diffusion coefficient.

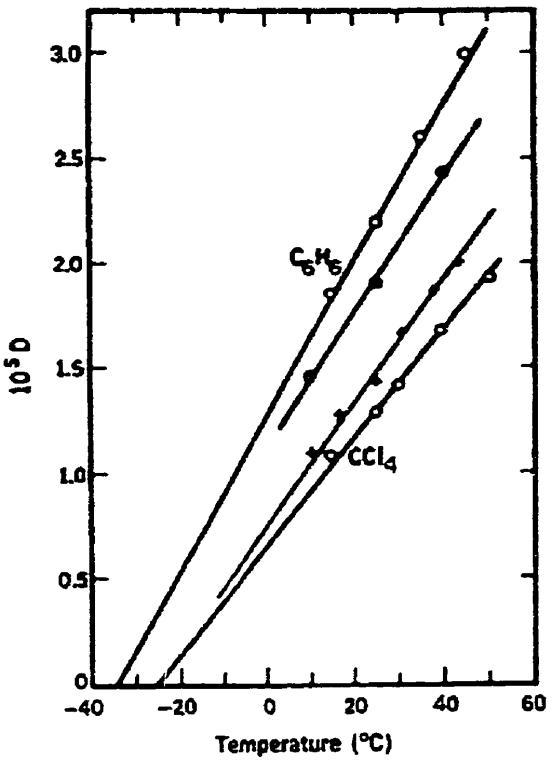

Figure 20 Diffusion Coefficient of C_6H_6 and CCl_4[36]

In Figure 20, the diffusion coefficients are expressed in cm^2/sec where the symbol "o" represents the self-diffusion coefficients of C_6H_6 and CCl_4, as shown near their corresponding lines. The symbol "•" represents the diffusion coefficient of CCl_4 in C_6H_6 while "+" represents the diffusion coefficient of I_2 in C_6H_6.

According to Hildebrand, approaching the problem of diffusion by way of viscosity makes diffusion a much simpler phenomenon. Various assumptions have been made in the past concerning the viscosity of liquids such as the assumption of quasi-lattice structure that ignores clear evidence to the contrary, or that the temperature dependence is exponential, or that there is an energy of activation which in fact disregards the basic distinction between liquid and plastic flow.[36]

As described by Hildebrand, the fact that a liquid can be so fluid and yet expanded so little over its intrinsic volume, is evidence of some of the unsound concepts that have been used by writers on transport theory. Some of these concepts are proposals that the trajectories between separable collisions, some of which are hard and others soft, and the presence of cages in which a molecule is oscillating with a definite frequency. During this time, it is awaiting an energy content which is in excess of the activation energy required to enable it to break through a barrier into a hole awaiting it at a distance of exactly one diameter. The fact that the mean free paths of molecules in simple liquids are much shorter than their diameters, led Hildebrand, in his work, to suggest that diffusion occurs by a succession of small displacements, not by leaps through barriers requiring energy of activation.[36] This theory appears to have similar elements to the fluctuation theory of Swalin[16] and Reynik [21]described earlier in Section 1.

To conclude, in an attempt towards a predictive theory, there is much evidence for a $D \propto T$ relationship for liquids, i.e., $D = KT$ and there is a need to evaluate "K" in terms of liquid/solute parameters for all systems.

5 Conclusions

While fully definitive statements are not available at this juncture, it appears that the results obtained to date support the following conclusions, namely:

1) The diffusion coefficient values with the "raw" g-jitter of MIR (corresponding to MIM latched) were similar to those obtained in similar alloy diffusion couples in 1992 on STS 47 and 52. Thus as far as liquid diffusion in narrow capillaries is concerned, both space vehicles provided similar reduced gravity environments.

2) The diffusion coefficient value may be reduced markedly by reducing the gravity field from 1g to that of the STS or MIR in low earth orbit.

3) The reduction of g-jitter, afforded by MIM, reduced the measured value of the diffusion coefficient even further, perhaps by another factor of 2 for the Pb-Au system.

4) The diffusion coefficient obtained with a larger specimen diameter (3 mm), and with MIM in latched mode, was somewhat larger than that of the equivalent specimen of smaller diameter (1.5 mm).

5) The experimental data obtained so far in the present study suggested a linear relationship between the diffusion coefficient and the temperature for both metallic and semiconductor alloys.

6) The use of the MIM on any manned space platform operating in low earth orbit (LEO) is essential when attempting to obtain accurate experimental values for liquid diffusion coefficients, even taking note

that MIM is ineffective in isolating the experimental facility from disturbances induced by "jitter" of less than 0.01 Hz. These more accurate diffusion coefficient values should permit a detailed examination of the current understanding of the structure(s) of liquid metals and semiconductors. Such an understanding should eventually permit the accurate prediction of the diffusion coefficient values for all alloy systems, a feat only possible as a result of the judicious use of LEO processing.

7) Low frequency, small amplitude (< 4 milli-g) single axis forced g-jitter does appear to induce appreciably increased liquid transport in narrow long capillary liquid diffusion specimens in the Pb-Au system.

6 Recommendations for Future Work

1) Complete the analysis of the remaining MIR-processed diffusion couples, particularly the ternary diffusion couples and the inter-diffusion couples.

2) It is strongly recommended that additional forced oscillation samples be processed to confirm the present results. Furthermore, the equivalent diffusion couples should be processed in the MIM latched and isolated mode under identical processing conditions. This will permit a better correlation between the effects of convection and g-jitter on the diffusion of liquids and hence, provide a more complete set of data.

3) Develop suitable semi-empirical potentials for the alloys of interest using the "embedded atom method".[37]

4) Conduct molecular dynamics simulations of liquid diffusion.

5) Examine the potential use of neutron diffraction to follow the atomic movements associated with liquid diffusion.

6) Replicate the experiment by Hildebrand using the concept of the hypodermic needles but with an array of very small diameter (1 mm) silica glass container for liquid metal diffusion experiments.

References

1. Smith R. W., Robert J., "Solute Diffusion in Dilute Liquid Metals and Metalloids", 11th International Symposium on Experimental Methods for Microgravity Materials Science, TMS Annual Meeting 1999, to be published.

2. Smith R. W. *et al.*, "The QUELD II – MIR Materials Processing Facility", 10th International Symposium on Experimental Methods for Microgravity Materials Science, TMS Annual Meeting 1998.

3. Frohberg G., Kraatz K. H., "Microgravity Experiments on Liquid Self and Inter-diffusion", Symposium Norderney, August 1986, p.27.

4. Vézina L. *et al.*, "NASA 7/QUELD – MIM Flight Data Analysis Test Report", Canadian Space Agency, St-Hubert, QC, August 1998.

5. Frohberg G., "Microgravity: A unique tool to discover new features of diffusion process", IN SPACE '93 Conference Proceedings, Oct. 5.

6. Frohberg G., Chapters V in "Fluids Sciences and Materials Science in Space", Ed. H. U. Walter, Springer-Verlag, Paris, 1987.

7. Frohberg G., Kraatz K. H., and Wever H., "Diffusion and Transport Phenomena in Liquids under Microgravity", Proc. 6th European Symposium on Materials Sciences under Microgravity Conditions, Bordeaux, France, 2-5 December 1986, (ESA 1987), SP-256, p.585.

8. Langbein D., "Materials Science in Space", Ed. B. Feuerbacher, H. Hamacher, and R. J. Naumann, Springer-Verlag, 1986.

9. Nachtrieb N. H., "Selfdiffusion in Liquid Metals", Proc. Int. Conf. on Properties of Liquid Metals, Ed. Adams, Davies, and Epstein, Taylor and Francis, London, 1967, p.2112.

10. Rosenberger F., "Fundamentals of Crystal Growth I", Springer-Verlag, 1979.

11. Kirkaldy J. S. and D. J. Young, "Diffusion in the Condensed State", The Institute of Metals, London, 1987, 527pp.

12. Einstein A., Ann. Phys., Leipzig, 1905, vol. 17, p.549.

13. Glasstone, S. K., Laidler K. J., Eyring H., "The Theory of Rate Processes", McGraw-Hill, New York, 1946.

14. Jost W., Diffusion in Solids, Liquids and Gases, 1960.

15. Cohen M. H., Turnbull D., "Molecular Transport in Liquids and Glasses", J. Chem. Phys., vol. 31, 5, November 1959, p.1164.

16. Swalin R. A., "On the Theory of Self-diffusion in Liquid Metals", Acta Met., vol. 7, November 1959, p.736.

17. Swalin R. A., "Diffusion in Liquid Tin", Acta Met., vol. 8,June 1960, p.388.

18. Frohberg G., Kraatz K. H., and Wever H., "Self-diffusion of Sn_{112} and Sn_{124} in liquid Sn", ESA SP-222, 1984, p.201.

19. Reynik R. J., "A Semiempirical Small Fluctuation Theory of Diffusion in Liquids", Trans. Met. Soc. AIME, vol. 245, January 1969, p.75.

20. Nachtrieb N. H., Petit J., "Self-Diffusion in Liquid Mercury", J. Chem. Phys., vol. 24, 4, April 1956, p.746.

21. Reynik R. J., Appl. Phys. Letters, vol. 9 1966, p.239.

22. Bruson A., Gerl M., "Diffusion Coefficient of ^{113}Sn, ^{124}Sb, ^{110m}Ag, and ^{195}Au in Liquid Sn", Phys. Rev. B, vol. 21, 12, June 1980, p.5447.

23. Protopapas, P., Andersen H. C., Parlee N. A. D., J. of Chem. Phys., vol.59, 1, 1973, p.15.

24. Shimoji M., Itami T., "Atomic Transport in Liquid Metals", Trans Tech Publications Ltd., Switzerland, 1986, 344pp.

25. Iida T., Guthrie R. I. L., "The Physical Properties of Liquid Metals", Clarendon Press, Oxford, 1988, 288p.

26. Zhu X., Ph.D. thesis, Queen's University, Canada, 1997.

27. Massalski T. B., "Bulletin of Alloy Phase Diagrams", vol.1-2, ASM International from Materials Park Ohio, 1992.

28. Ozelton, Swalin R. A., Phil. Mag., vol. 153, 18, 1968, p.441.

29. Paoletti, Vicentini, J. of Appl. Phys., vol.32, 1, 1961, p.22.

30. Zhu X., Smith R. W. , "Diffusion in Liquid Pb-Au Binary System", Materials Science Forum, Transtec Publications, vols. 215-216, 1996, p.113.

31. Hinchcliffe S., 4thYear Project, Queen's University, Department of Materials and Metallurgical Engineering, 1997.

32. Perkin-Elmer Manual: Analytical Methods for Atomic Absorption Spectrophotometry, The Perkin-Elmer Corporation, 1982.

33. Thompson W. T., Materials Science Laboratory Manual, RMC, 1995.

34. Zhu X., Smith R. W., "Impurity Diffusion of Gold in Liquid Lead", Adv. Space Res., Elsevier Science Ltd., vol.22, 8, 1998, p.1253.

35. Griesche A., Kraatz K. H., Frohberg G., "A Modified Shear Cell for Mass Transport Measurements in Melts", Rev. Sci. Instrum., American Institute of Physics, vol.69, 1, January 1998, p.315.

36. Hildebrand J. H., "Viscosity and Diffusivity", Wiley-Interscience Publication, New York, 1997, 109 pp.

37. Foiles S. M., Baskes M. I., Daw M. S., "Embedded-atom-method Functions for the fcc Metals Cu, Ag, Au, Ni, Pd, Pt, and their alloys", Phys. Rev. B, vol.33, 12, June 1986, p.7983.

Appendix I

excerpt from "The QUELD II – MIR Materials Processing Facility"
by Smith R. W. et al.[2]

QUELD II Facility

In order to attempt to ensure a trouble-free extended lifetime for QUELD II in space, the conceptual design drew heavily on the most relevant aspects of the space-qualified and flight-proven QUESTS I and QUELD I units. QUELD I had been used solely for isothermal processing and since the operating astronauts had to select the operating temperatures manually and change the temperature setting immediately after inserting the samples, two single zone furnaces were used. However, QUESTS I was an automated facility with three-zone furnaces, sample-quench facilities and could be used for isothermal and gradient-freeze sample processing. The QUESTS furnaces and quench system had also been used in a rocket-born materials processing facility which contained 14 of the furnace units. In all cases the furnaces and quench block systems had performed as required and so give confidence that they could be used with some high level of confidence for extended use on MIR in order to process various types of samples. To do this, the astronaut/cosmonaut would have to select the sample from a storage magazine, insert it in the sample carrier, enter the sample identity number and press the start button. Following this they would be processed automatically in one of the three modes:

1) isothermal
2) temperature-gradient
3) gradient-freeze

The scientific programme carried-out to date has exploited capabilities of QUELD II in all of these three modes.

The QUELD II system processes samples via the automatic insertion of the sample into a preheated furnace. The furnace temperature is controlled via a programmed temperature controller. Following the required thermal exposure, the samples are automatically withdrawn and are subsequently quenched by the automatic closure of paired spring-loaded quench blocks. Once the samples are at a safe handling temperature, the samples are released by the quench mechanism and await manual removal from the hardware.

All sample processing routines are contained within a removable memory module. A single module contains the information necessary to process approximately 50 different samples. The specific sample routine is defined using two digit selector switches on the front panel of the QUELD II hardware.

The capacity of the QUELD II system is enhanced by the use of two fully independent sample processing channels. Due to power limitations on MIR, only one channel is in operation at any given time, however, it is possible to load both channels at the same time and make use of a preprogrammed time offset to sequence the processing routines for each sample and so reduce demands on astronaut/cosmonaut time by only requiring their attention for reloading samples after every second sample has been processed.

THE SAMPLE

A. Specifications

The QUELD II system has as its focus the accurate thermal processing of a wide series of specimen-types. Each type of specimen must be encased in a protective metallic container to permit processing without hazard for the operator or the equipment. The whole assembly is referred to as a "sample". A schematic drawing of a typical sample is shown in Figure I-1. Its specifications are shown in Table I-1.

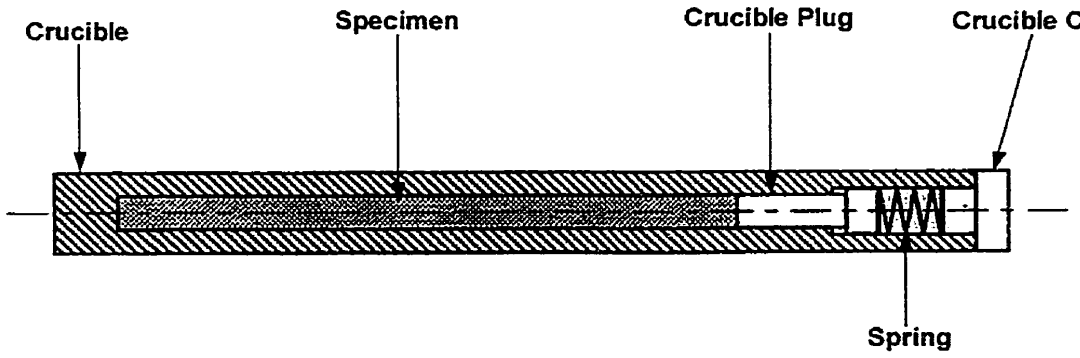

Figure I-1 Schematic Diagram of a Typical Crucible

Table I-1: Listing of the Primary Specifications for QUELD II Experimental Samples

Parameter	**Description**
Nominal Sample Diameter	6.4 mm
Nominal Sample Length (Including Mounting)	157 mm
Nominal Crucible Diameter	5.4 mm
Maximum Crucible Length Including Cap	60 mm
Nominal Crucible Wall Thickness	0.6 mm
Nominal Specimen Diameter	4 mm
Material Sheathing	321 Stainless Steel or 601 Inconel
Crucible Material	Pyrolitic Carbon or Boron Nitride

B. Chemical Containment

The requirements for containment are that the specimen, when liquid, does not reach beyond its immediate environment and that none of the specimen constituents are permitted to leak into the QUELD II flight unit or elsewhere. This requires that the specimen be contained in a suitably inert crucible, closed with a spring loaded plug to ensure that no free surface exists during microgravity processing to avoid any potential Marangoni convection.

The selection of the crucible and sheathing materials was based on meeting the requirement that the specimen materials, when in the liquid state, do not seriously affect the crucible or sheathing materials' integrity when exposed in direct contact for a period of at least twice the duration of the planned experiment.

C. Structural Containment

The materials and assembly techniques selected for the sample must be able to withstand the internal loading likely to arise within the capsule in the unlikely event of a furnace run-away condition. For the QUELD II, this required that the entire sample must be able to withstand a temperature of 950^{0}C for 10 hr. As a result, duplicates of all sample types are routinely tested in this manner. In practice, in order to be accepted for microgravity processing, all specimens must be enclosed in two impervious sealed shells. Metallic diffusion couples are best placed first in a graphite or boron nitride crucible and then sealed by laser welding in two vacuum-tight layers of stainless steel. Springs are included not only to prevent Marangoni convection within the crucible but also to gently force the crucible to make good thermal contact

at its base with the central steel plug of the stainless steel envelope. This permits the user to place a thermocouple through a hole drilled in the plug to within 1 mm of the inner crucible in order to obtain confirmation that the processing temperature at that point is closely similar to that obtained during the ground-based testing. While it is recognized that the temperature measured in the plug by the external thermocouple will be below the value of that existing at the actual base of the specimen, ground-based testing with thermocouples mounted in the actual specimen permit a close reproducible correlation of the two temperatures.

Should the nature of the specimen permit sealing in quartz, then only one level of protective stainless steel needs to be used, thus permitting a larger specimen size.

Following laser welding, the samples are subjected to a series of tests. The first of these involves taking a duplicate sample of each type and exposing it in a furnace at 950^{0}C, in air, for 10 hours. If the protective metallic container is still fully protective after this exposure, the containment technique is deemed adequate from a toxicological point of view.

Then the intended flight samples are examined by X-radiography to ensure the required specimen and sample components are in place. Finally, each flight sample is subjected to a "leak-detection" test in which the welded sample is first placed into a vessel under alcohol at a pressure of 50 p.s.i. in order to force a volatile fluid into any micro cavities existing in the stainless steel case. Following this, the sample is surface-dried and placed in vacuum system, which is then sealed. The time taken for the pressure in the vacuum system to fall to a given value is then measured. If the steel case is perforated due to incomplete welds or other manufacturing defects, the

rate of reduction of pressure is much reduced and so the sample condition can be identified to be "leaking" or "suspicious" and returned for re-manufacture. Following the successful passing of the leak test, the sample is ready for flight testing.

QUELD II FEATURES AND SPECIFICATIONS

The key features of the QUELD II system are:

- Maximum operating temperature of 900°C
- Maximum temperature gradient of 70°C/cm
- Isothermal and temperature gradient exposure profiles
- Twin independent channels for increased processing capacity
- Three-zone furnace windings for control of thermal gradients
- Required astronaut crew time of only 5 minutes per double sample selection and exchange
- Automatic sample insertion into a preheated furnace to more rapidly bring the sample to the desired operating temperature
- Automatic sample quench
- Complete sample process information set by a two digit code on front panel
- All sample processing codes present on replaceable memory modules

In addition to the above, there are several advantages to the combination of the QUELD II system with the MIM platform (as described in Appendix II). It is noted that the MIM may be used in three modes:

1. "Latched": In this condition, the MIM g-jitter of the platform on which MIM is mounted is passed directly to QUELD II.
2. "Isolating": Here, the ability of the MIM to improve the quality of the microgravity environment to a quiescent level of 10^{-6} g permits, for example, the collection of high fidelity thermophysical data.
3. "Forcing": In this mode, the MIM continues to isolate the QUELD unit from local g-jitter but then forces the platform to vibrate in desired manner.

This ability of the MIM to generate controlled microgravity fluctuations not only permits the study of the effects of gravity on physical processes, particularly the triggering of interface instabilities, but also allows the operator to conduct experiments designed to refine the theoretical understanding of the effects of gravitationally-induced convection. For example, it may be reasoned that when a given sample is subjected to a particular vibration pattern, then certain convection should result, leading to a particular solute redistribution in a growing crystal. The experiment can be carried-out and the resulting solute distribution determined. This is then compared with that predicted and, if these do not correspond, then the theoretical prediction is modified to better reflect the fact. The final advantage of the MIM/QUELD combination is that the available data transfer ports on the MIM permit the recording of experimental parameters important in the post-mission analysis of sample properties. The capacity to do this is large since the MIM uses an optical disk storage system. Figure I-2 is an illustration of the QUELD II system installed above the MIM unit.

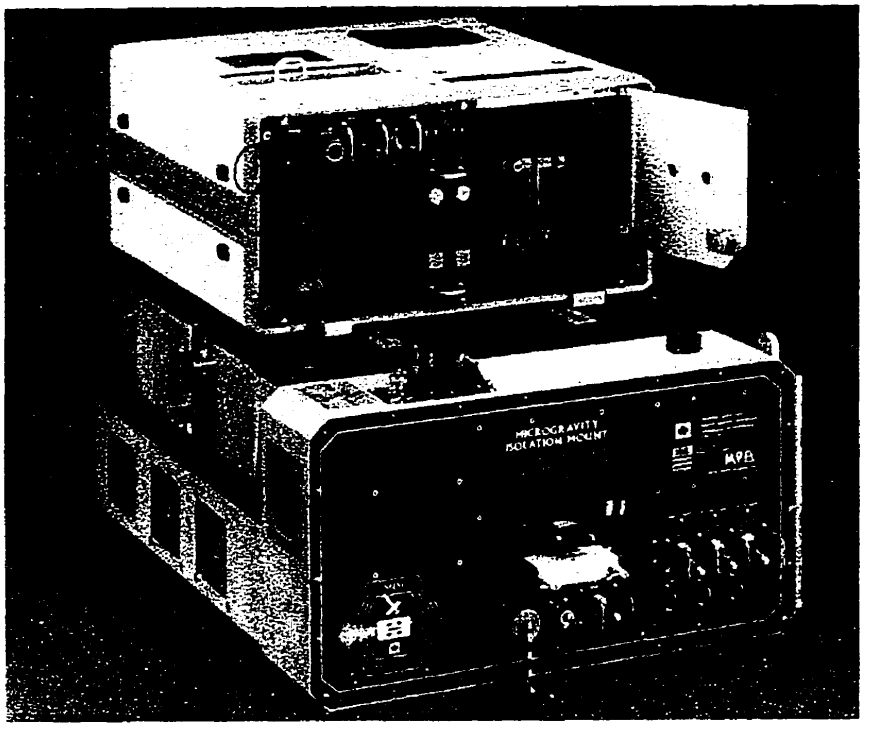

Figure I-2 QUELD II System installed on MIM

SCIENCE SUPPORT CAPABILITIES

As noted earlier, samples may be processed isothermally, in a fixed temperature gradient, or in the falling temperature gradient characteristic of the gradient-freeze crystal growth process. This permits a wide range of science objectives to be achieved. The following is a summary of the science activities carried-out this far.

A) Liquid Diffusion

A series of dilute binary and ternary diffusion couples have been processed to determine the diffusion coefficients for a particular set of temperatures and examine how these change with the processing temperature. The former is of direct use in the mathematical modelling of industrial processes involving liquid metals while the latter provides fundamental knowledge with respect to the structure of liquids.

These experiments are best done in a microgravity environment since buoyancy convection is much reduced and so more accurate data may be obtained. When these are done, using the Microgravity Isolation Mount (MIM) in "Isolating Mode", then even better data has been obtained. In work carried-out to date, g-jitter has been shown to increase the measured diffusion coefficient of gold in liquid lead by a factor of two.

B) Ostwald Ripening in a Molten Salt Medium

When a fine dispersion of a given medium contained within another is exposed at high temperature, it is usually found that the larger particles coarsen (or ripen) at the expense of the smaller ones such that, over time, the fine dispersion becomes completely replaced by one of larger particles. This phenomenon, examined by Ostwald at the turn of the last century, is of critical importance in many technological areas and, so, much work has been done to try to obtain a better understanding of the associated kinetics. If such experiments are performed in space, buoyancy effects are removed and in so doing, liquid/solid and liquid/liquid systems may be studied.

In the present MIR/MIM/QUELD II campaign, both the ripening of a liquid/solid and a liquid/liquid system have been studied in the presence and absence of g-jitter.

C) Processing of Heavy Metal Fluoride Glasses

The overall objective of this work is to realize the predicted ultra-low losses for infra-red radiation transmission in heavy metal fluoride (HMF) glass fibres by processing in microgravity. Empirical studies have shown that glasses cooled in microgravity are less susceptible to devitrification. Hence, various glasses will be processed using the MIM to help towards obtaining a better understanding of why this occurs. Such glasses, when drawn to fibres, achieve a very high value-added status and have many application, particularly for military use.

D) Solute Partitioning in InSb and GaSb

In the growing of semiconductor crystals with controlled doping it is essential that the manner in which solute partitions between the solid and the contiguous liquid be known precisely. However, the accurate determination of such partition coefficients in a terrestrial laboratory is plagued with error due to buoyancy effects. Hence the QUELD II facility has been used in a gradient freeze mode to permit crystal growth under diffusion-controlled conditions of binary and tertiary compound semiconductors. The MIM is being used to determine the influence of g-jitter on such solute transport processes.

DESCRIPTION OF QUELD II MICROGRAVITY FURNACE

Physical Layout

The design of the QUELD II system is based on the use of the original QUESTS I furnace core design with three-zone temperature control, in combination with standard industrial subassemblies appropriately rated or upgraded for space flight qualification.

The essential features of the flight hardware are:

- Aluminum enclosure
- Modular CPU/process controller
- Interface backplane for I/O modules
- Replaceable memory module containing sample processing profiles
- Aluminum enclosure "plug-in modules" to contain furnaces
- DC drive linear actuators for sample insertion
- Paired quench blocks operated via linear actuators
- Mounting plates to interface with MIM

Internal Layout

The internal layout of the hardware is shown in Figure I-3. The CPU/process controller and complementary I/O modules plug directly into a rigid backplane designed specifically for use with the process control units. This backplane contains all the necessary communication hardware and wiring between the units. The

backplane is in turn securely mounted to the structural rails of the enclosure. The furnace plug-in module which contains the two furnace cores is inserted to one side of the enclosure and is secured in place using standard mounting hardware. The linear drives and quench block assemblies are mounted to a subframe that is fastened to the structural rails of the enclosure. Sample insertion and removal is performed by extensions from twin linear drives mounted below the furnace module. The front panel of the enclosure contains all the user interface components required for operation by the astronaut, plus access to the sample mounting locations.

QUELD II

Top View — Cover Removed

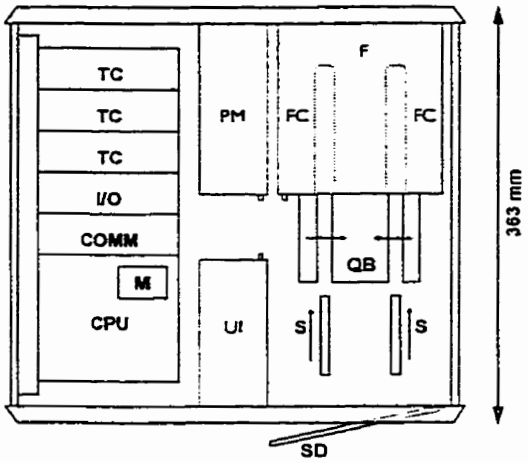

Legend

C	-Controls
CPU	-Central Processing Unit
COMM	-Communication Module
EM	-Electric Motor
F	-Furnace
FC	-Furnace Core
I/O	-Input/Output Module
LS	-Linear Slide Mechanism
M	-Memory Module
PM	-Power Control Module
QB	-Quench Blocks
S	-Sample
SD	-Sample Door
SS	-Sample Selector
TC	-Temperature Control Module
UI	-User Interface Module
——	-Motion of Component

Note: Access to Memory Module via top panel

Front View

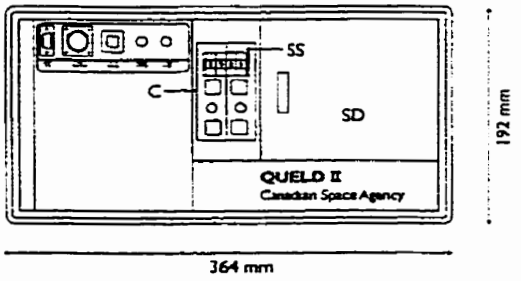

Layout of Sample and Furnace

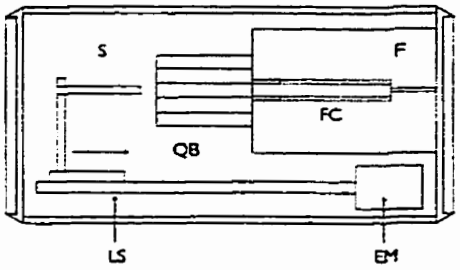

Features

- Automated Sample Processing
- Minimal Operator Time
- Process Parameters on Memory Card
- Robust Modular Design

Canadian Space Agency
Queen's University
Millenium Biologix Inc.

Figure I-3 Internal Layout of QUELD II

Appendix II

excerpt from "Solute Diffusion in Dilute Liquid Metals and Metalloids"
by Smith R.W. and Robert J.[1]

MIM Facility

The Microgravity Vibration Isolation Mount (MIM) is a six degree of freedom (6DOF) magnetic levitation (MAGLEV) system designed to isolate experiments from the vibratory accelerations (>0.01 Hz) on the space shuttle, MIR and ISS, while passing the quasi-static accelerations (<0.01 Hz) to the experiment. Given the typical 2 μg steady state acceleration in low earth orbit, the system is capable of isolating an experiment of practically unlimited mass, providing attenuation of the acceleration levels of up to 60 dB, thereby providing the desired low jitter acceleration environment to experiments. The performance limit depends primarily on the character of the umbilical required between the MIM base and the MIM flotor on which an experiment is mounted. The emphasis with the MIM design is to isolate at the experiment level, ideally isolating only the sensitive elements of an experiment. This limits the need for a heavy umbilical. In the current implementation, the umbilical provides power to the experiments mounted on the flotor, and provides data acquisition and control services to the experiments. With the wire umbilical, the MIM has demonstrated good isolation performance in operations on the MIR space station.

The MIM may be viewed as consisting of two major components: the fixed stator and the free flotor. The MIM achieves isolation in six degrees of freedom (6 DOF) using eight Lorenz actuators. These actuators consist of permanent magnets on the flotor interacting with coils mounted on the stator. The control system tracks the

flotor motion in 6 DOF and the flotor and stator accelerations in the three linear DOF, and determines the currents required in each of the coils such that full 6 DOF control of the flotor is achieved. For tracking the position and attitude of the flotor with respect to the stator, three light emitting diodes (LED) mounted on the flotor are imaged onto three 2-D Position Sensing Devices (PSD) mounted on the stator. This provides position tracking of the flotor with respect to the stator with a resolution of the order of 10 μm linearly and of the order of 10^{-4} radians rotationally. The MIM provides for a range of motion of approximately 9 mm in the three linear DOF and 3.5 degrees in the three rotational DOF about its nominal home position. The MIM operating parameters are given below.

MIM OPERATING PARAMETERS

MIM Operating Parameters

Volume:	1 MLE (Mid-deck Locker Equivalent)
Total System Mass	54 lb (Estimate)

Power Requirements (Excluding experiments, PGSC and MOD):

Nominal power	106 Watts
Peak power in driven mode	120 Watts
Maximum touch temperature	Less than 40°C

Experiment Support

Mounting Surface Dimensions	36.2 cm x 36.2 cm (14.25 in. x 14.25 in.)

(Experiment hardware can overhang this where space is available)

Volume available on STS-85	Approx. 1 MLE

Isolated Mass	Volume limited only
Experiment Power	10A @ 28 VDC derated per NSTS-21000-IDD-MDK
Analog data channels	9
Channel Input Gains	1
Input range	+/- 10 Volts
Resolution	16 bit
Data Sampling Rates	500 to 1500 samples/sec/channel
Anti-Aliasing Filters	Fourth order Butterworth analog filters set at 100 Hz
Digital filtering/Decimation	Available from 1.0 Hz to 100 Hz range with storage rate from 5 s/s to 1000 s/s
Data Storage	2 Gbytes on MIM hard drive with SCSI port for transfer to external storage medium
Experiment control lines	8 analog output, 16 bit resolution, +/- 10 V 100 Hz response
Data Down-link	Data transfer via the OCA
Isolation Frequency Range	0.01 Hz to 100 Hz
Frequency Response	Second order and fourth order roll off achieved above cutoff frequency depending on control algorithm

Experiment Support Continued

Maximum attenuation	60 dB at 0.5 Hz and above limited by noise floor
Noise Floor	1 (micro-g)^2/Hz above 0.5 Hz (TBD)
Acceleration Range	17 mg depending on frequency and rattle space constraints
Acceleration Accuracy	10 micro-g
Acceleration Resolution	1 micro-g
Programmable g inputs	
Frequency Range	DC to 50 Hz
Motion Range	+/- 8 mm (+/- 0.3 in)
Maximum Force	5N (1.1 lb wt) in vertical direction and 2.5N (0.55 lb wt) in the horizontal direction

Typical MIM Data Plots for the Isolated and Forced Modes

For each acceleration plot, four values are presented: the mean, the minimum, the maximum and the standard deviation for 1 minute of recorded data which corresponds to 7500 data points. The accelerations are in milli-g (10^{-3}g) and the time scale is in minutes.

In the QUELD experiments, the samples are often processed in sequence. This means that there are usually two samples processed for each raw data file, one sample

after the other. Therefore, the first part of the plot represents the first sample, and the second part, the second sample.

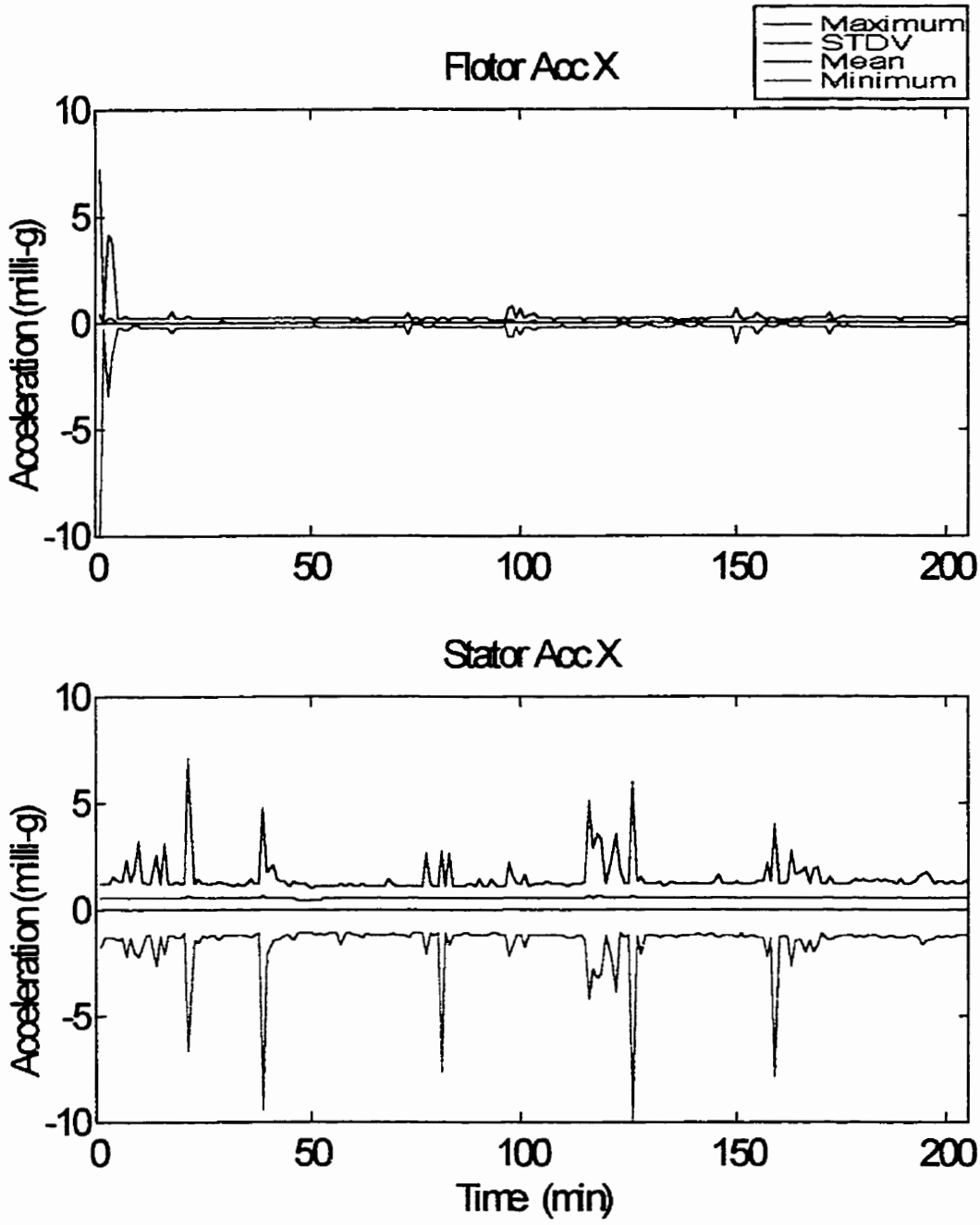

Figure II-1 Samples 63 and 64 in the Isolated Mode for X-axis

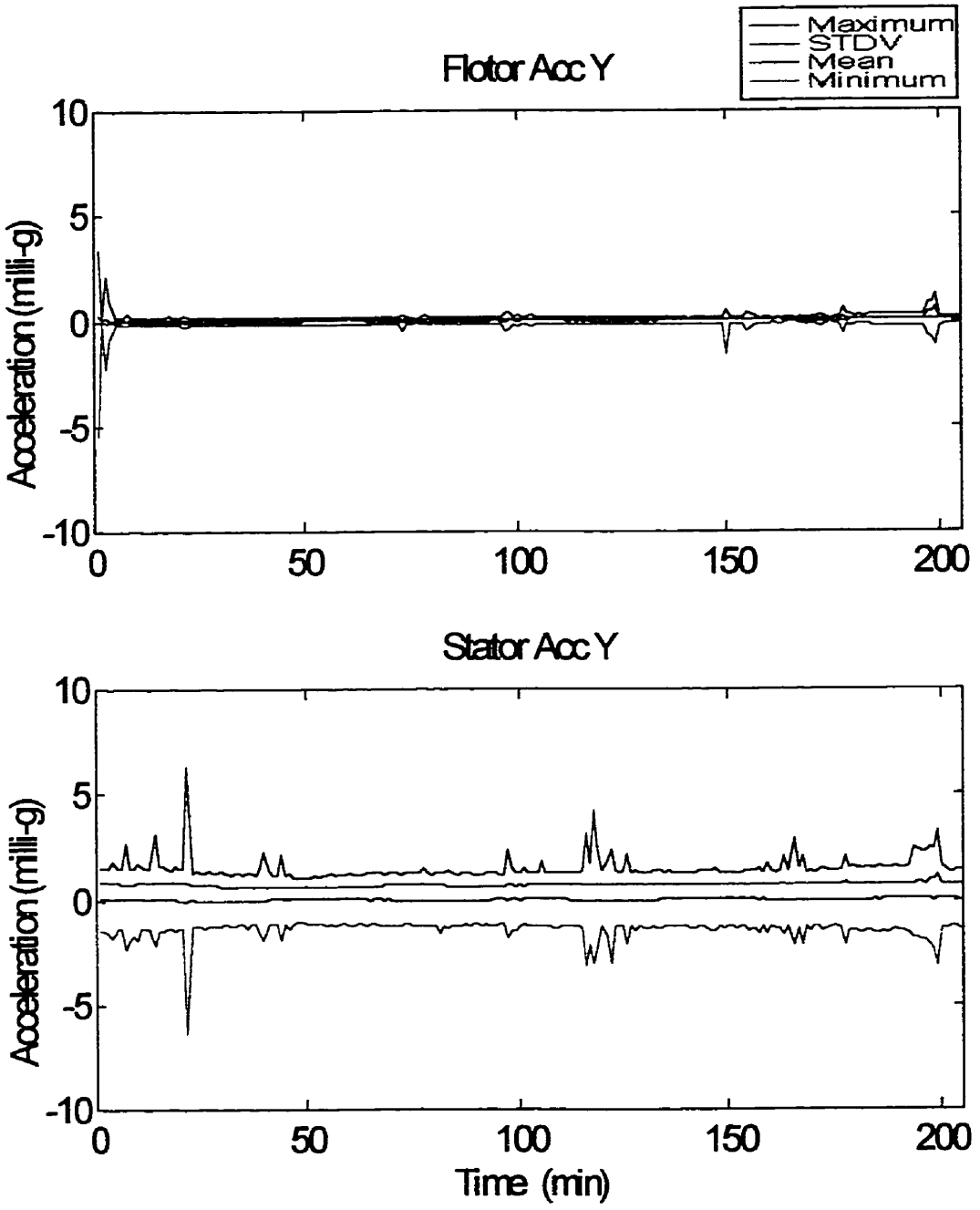

Figure II-2 Samples 63 and 64 in the Isolated Mode for Y-axis

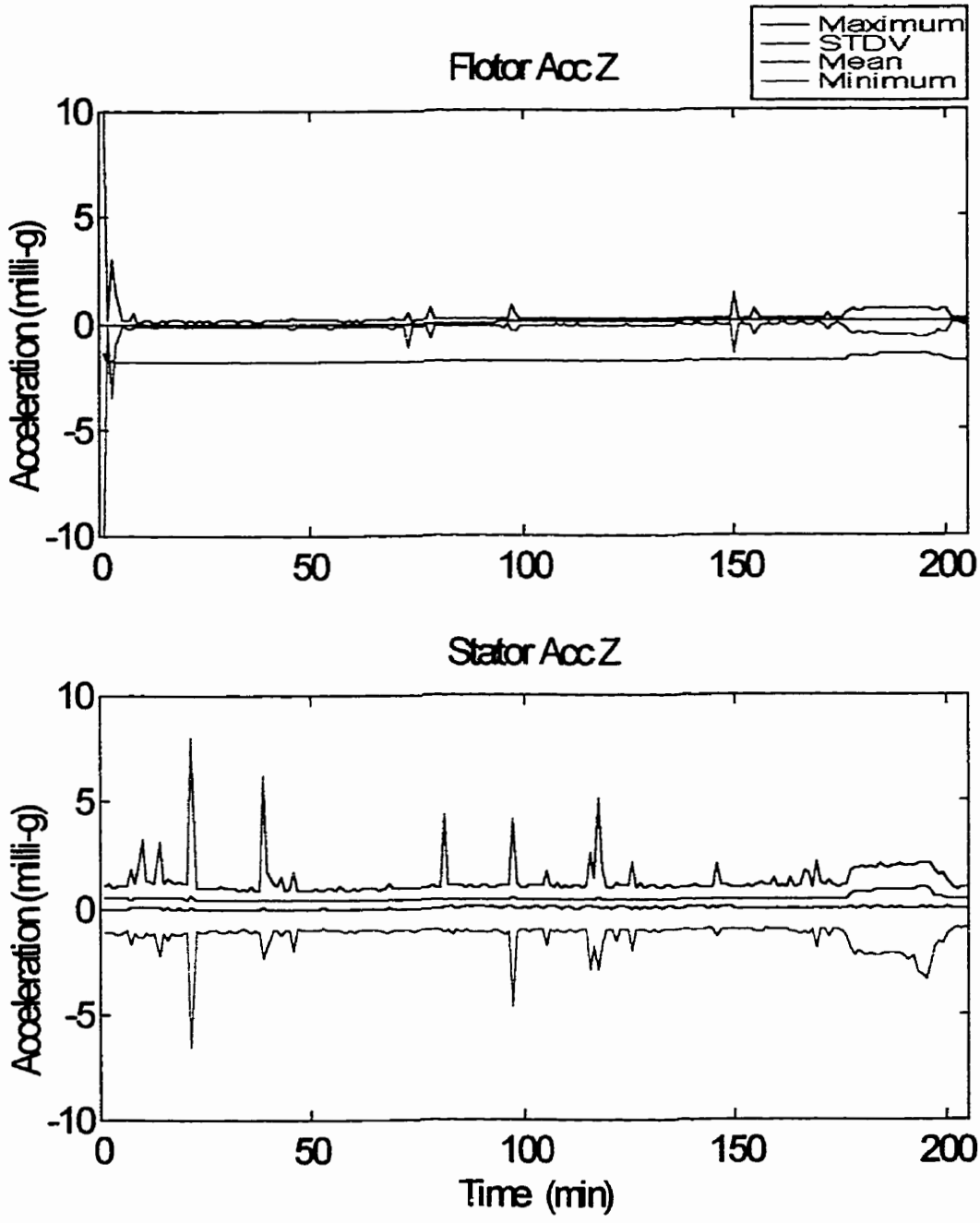

Figure II-3 Samples 63 and 64 in the Isolated Mode for Z-axis

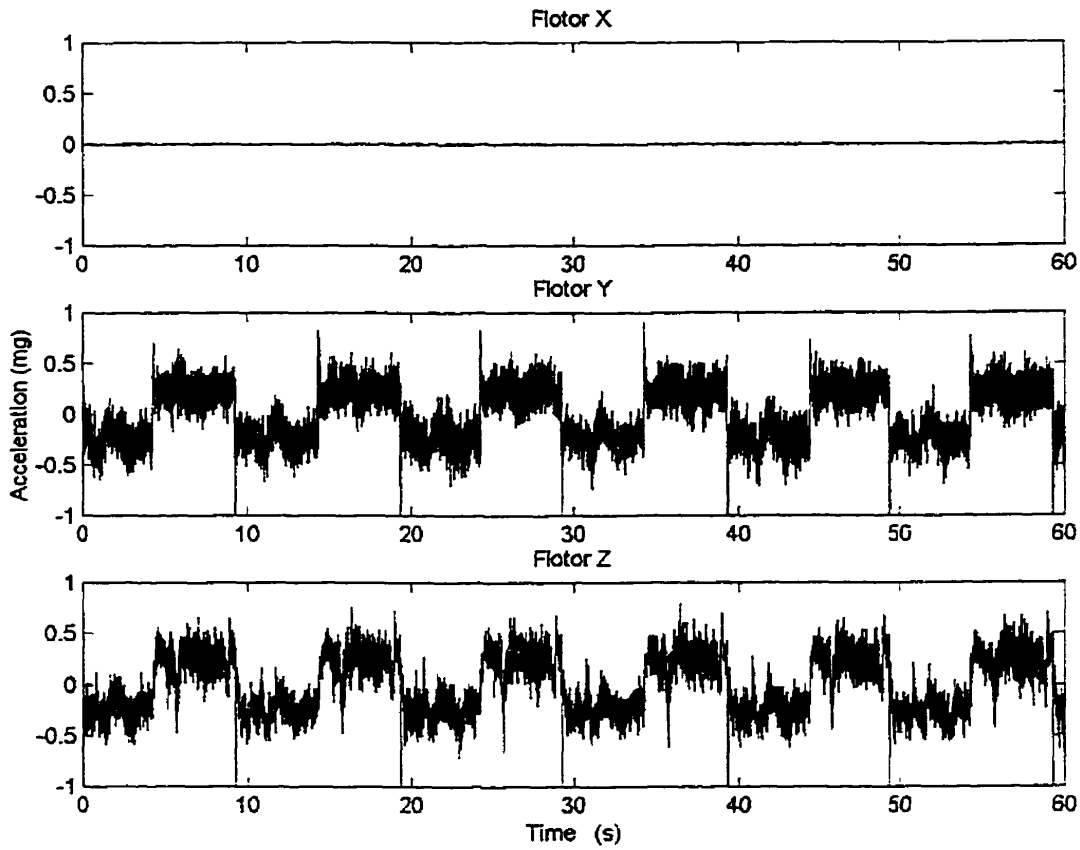

Figure II-4 Samples 401 and 402 in the Forced Mode for the Flotor at Time=30 min.

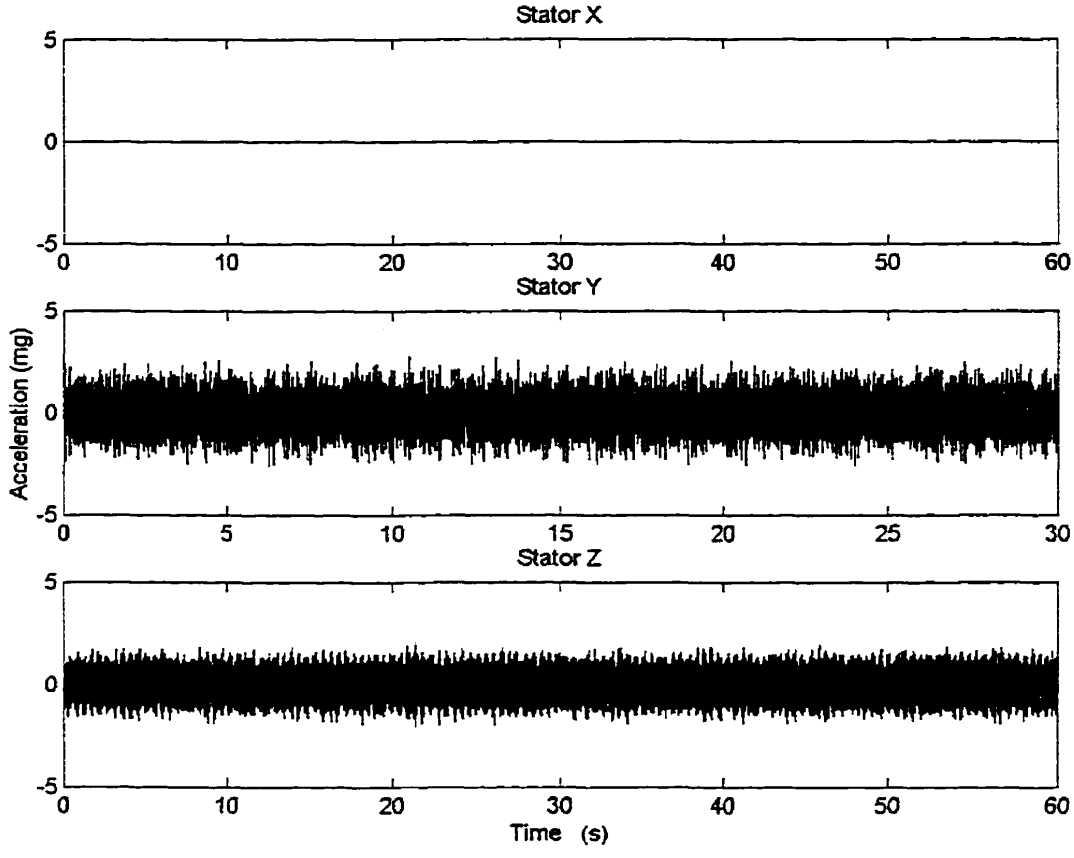

Figure II-5 Samples 401 and 402 in the Forced Mode for the Stator at Time=30 min.

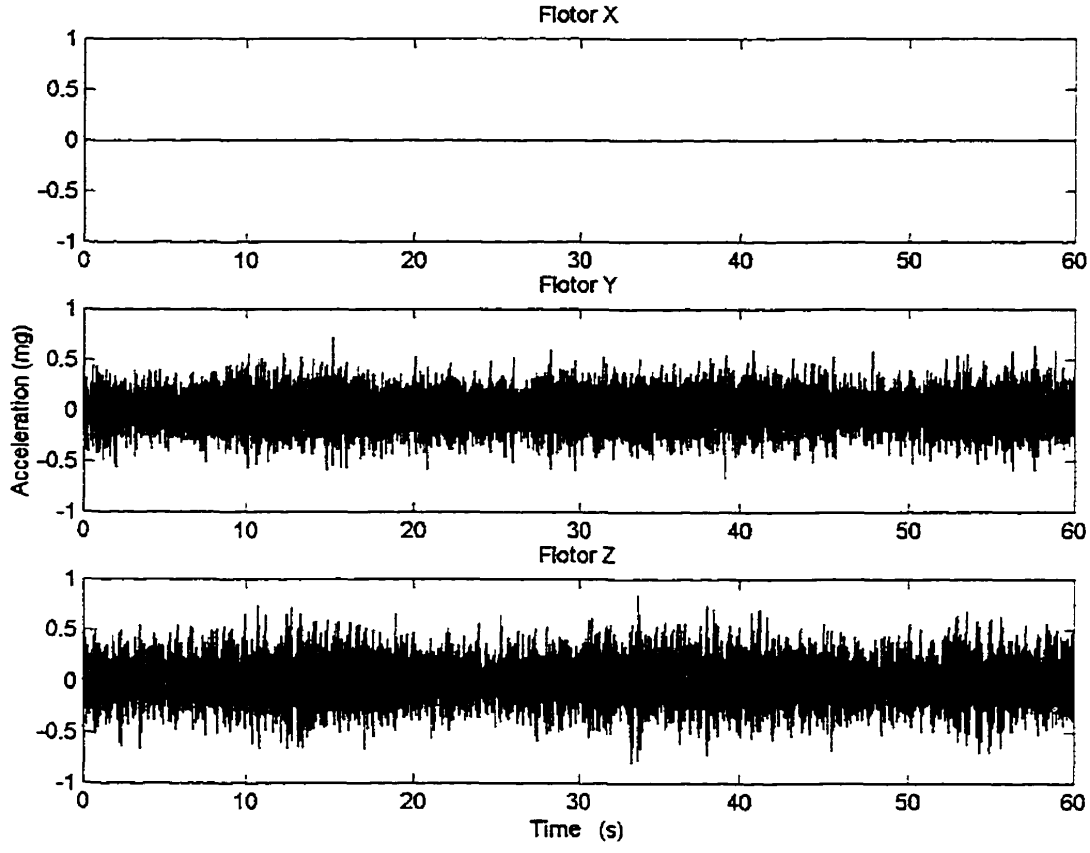

Figure II-6 Samples 419 and 420 in an Unconfirmed Latched Mode for the Flotor at Time=10 min.

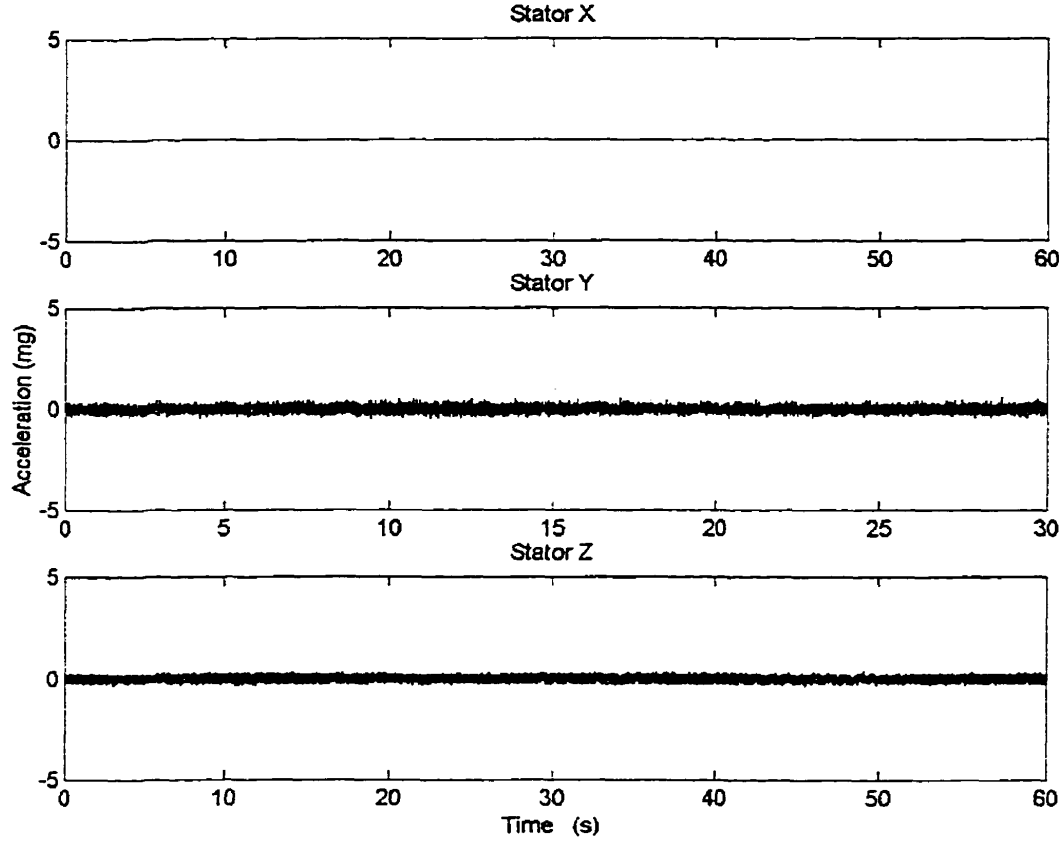

Figure II-7 Samples 419 and 420 in an Unconfirmed Latched Mode for the Stator at Time=10 min.

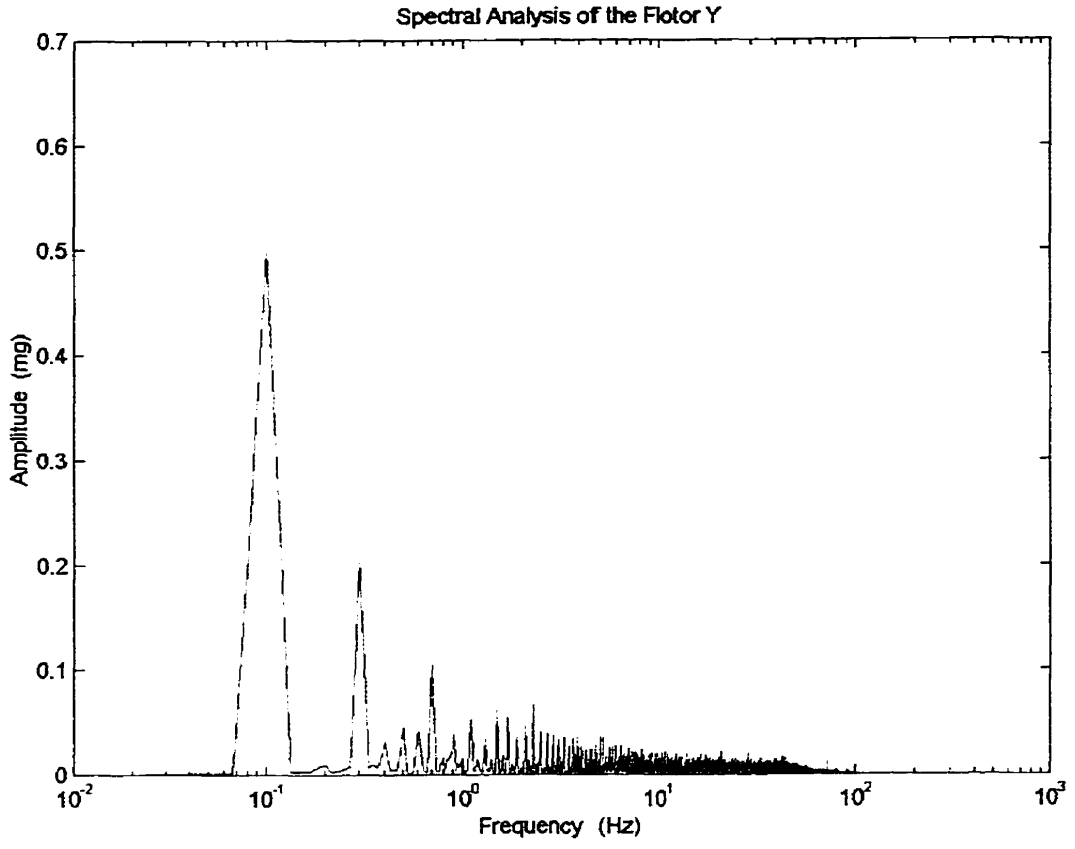

Figure II-8 Typical Spectral Analysis of a Sample in the Forced Mode

As it can be seen in Figures II-1 to II-3, the MIM effectively isolates the Flotor from the Stator. These acceleration plots are representative for all the samples that were processed in the isolated mode of the MIM. Figures II-4 and II-5 shows the capability of the MIM to isolate the flotor from the stator and induce a forced oscillation of 0.1 Hz at 45° to the sample axis.

Samples 419 and 420 were initially believed to have been processed in the isolated mode but after verification of the MIM data logs and the astronaut logs, it was concluded that they were in fact processed at an unconfirmed latched mode, since

Figures II-6 and II-7 are similar. However, since the MIM mode can not be confirmed, the diffusion coefficients were omitted in the results section of this thesis.

Finally, from Figure II-8, one can observe that, based on the spectral analysis, the MIM was oscillating at a frequency of 0.1 Hz. All the samples processed at a forced oscillation were investigated in this manner to verify the proper operation of the MIM.

Appendix III

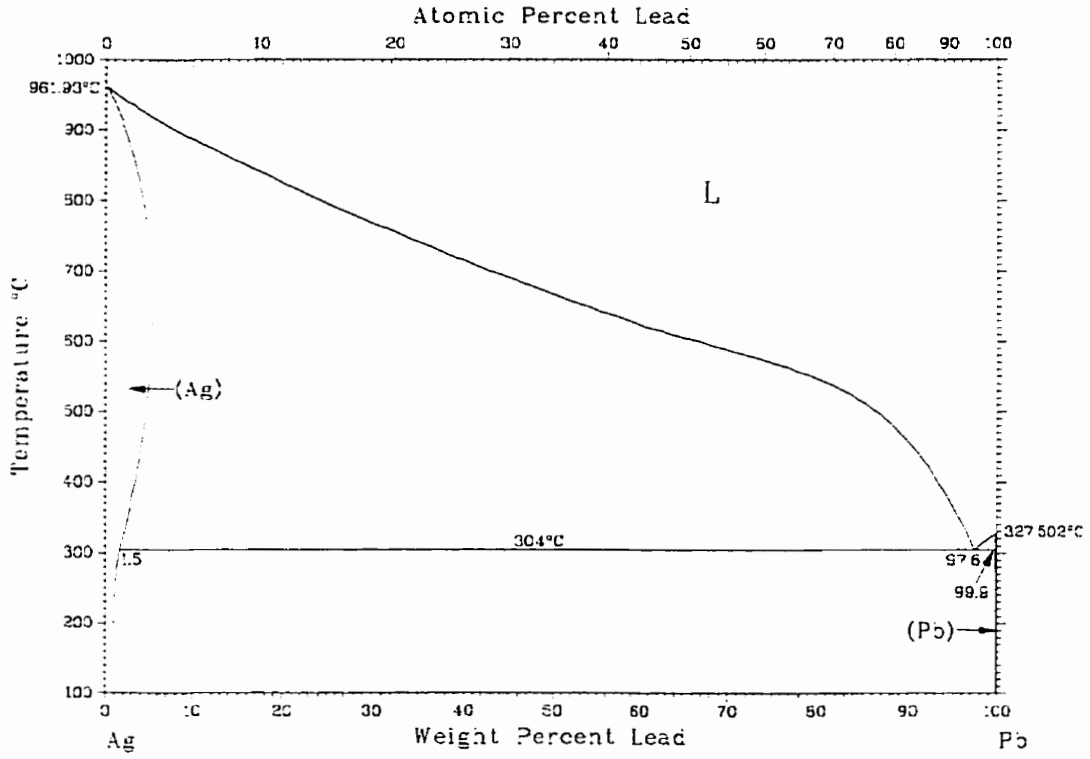

Figure III-1 Silver-Lead Binary Phase Diagram

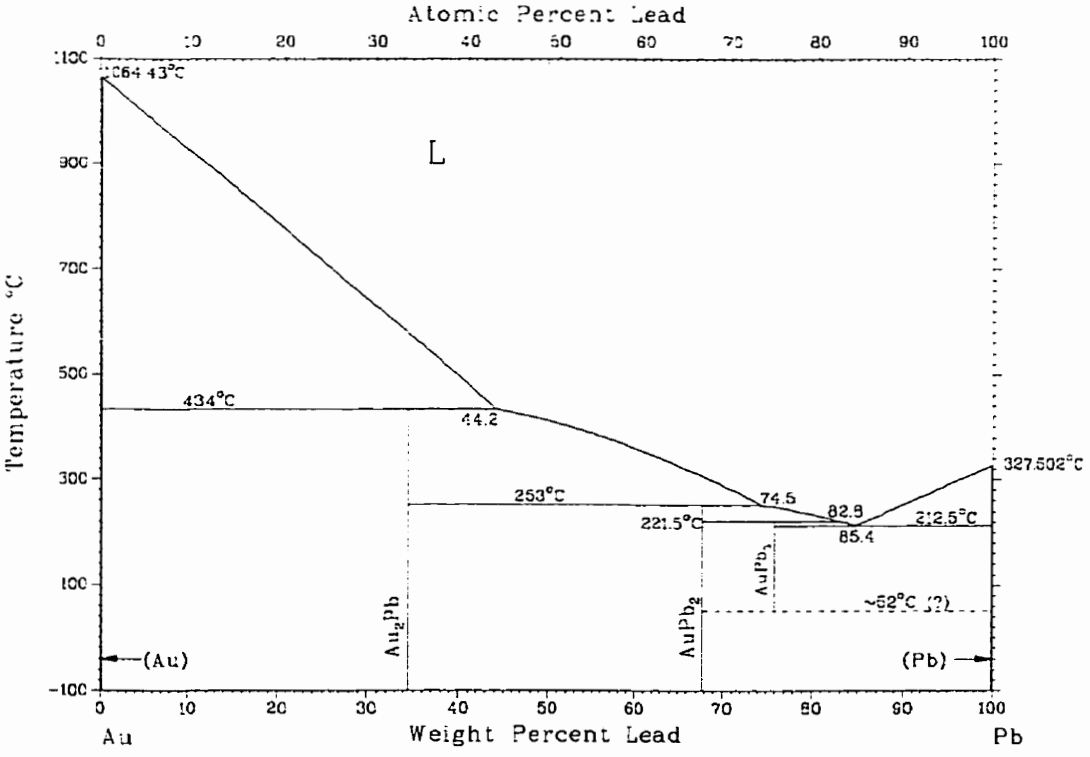

Figure III-2 Gold-Lead Binary Phase Diagram

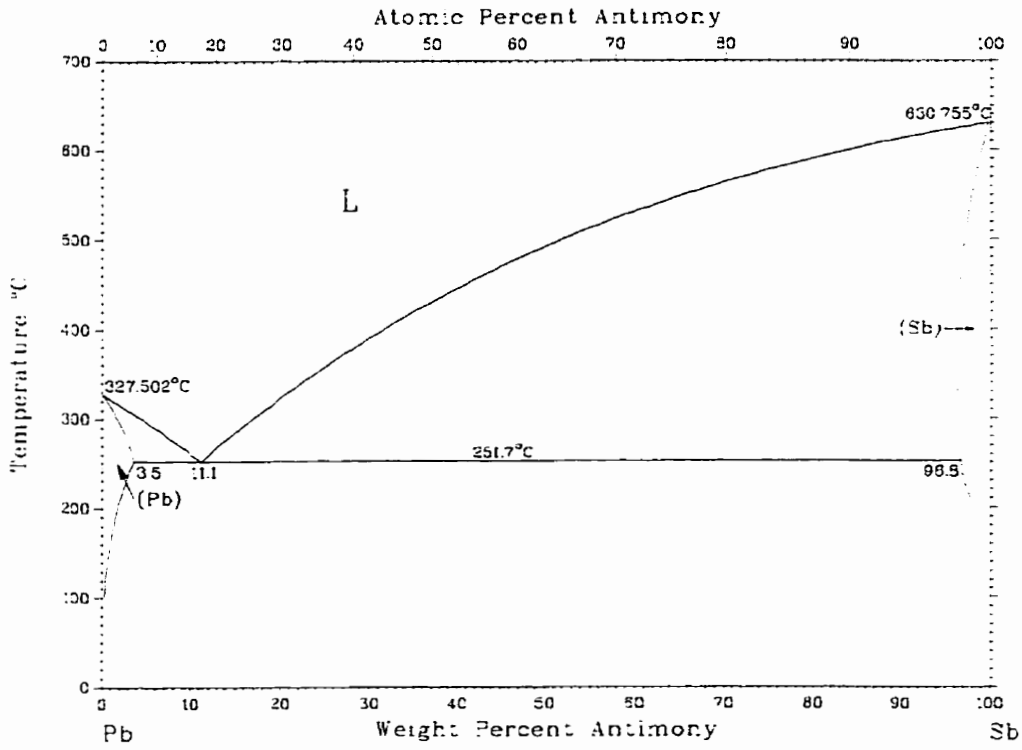

Figure III-3 Lead-Antimony Binary Phase Diagram

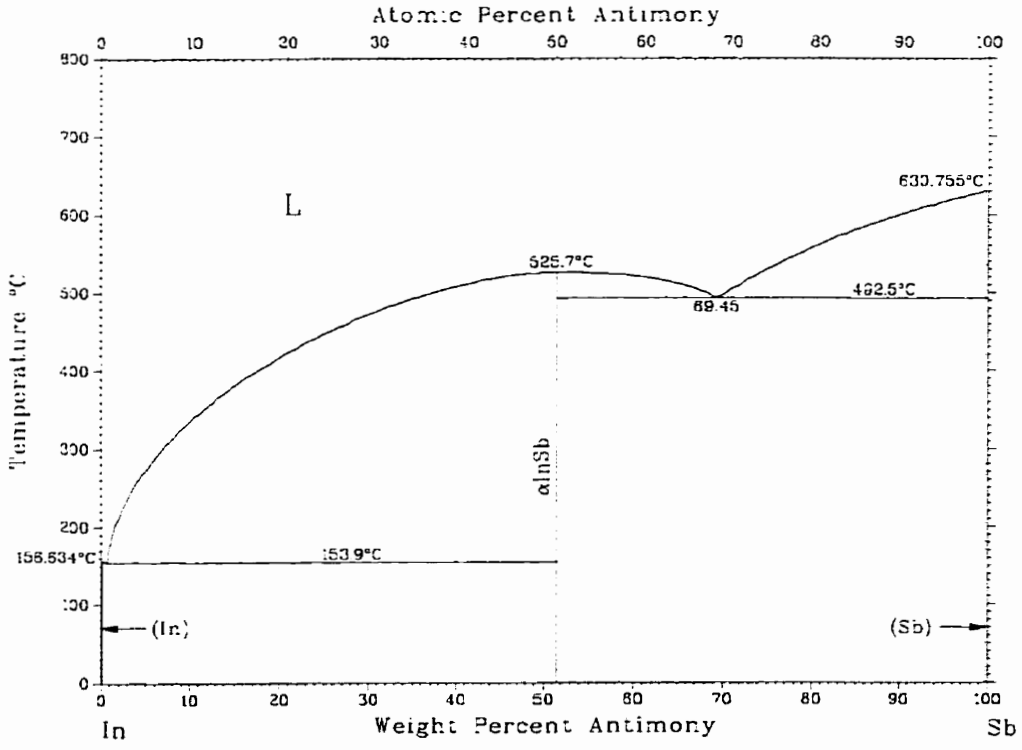

Figure III-4 Indium-Antimony Binary Phase Diagram

Appendix IV

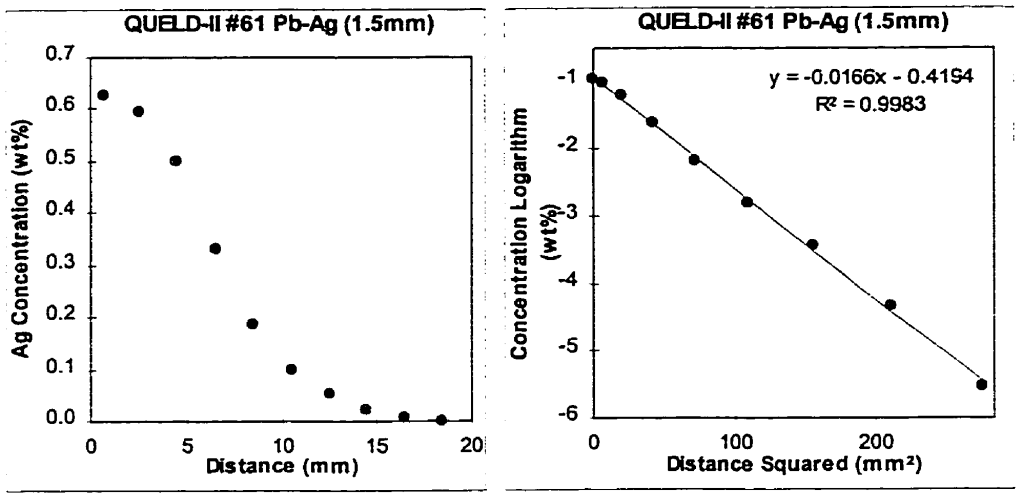

Figure IV-1 Concentration Profile and Regression Analysis of Sample #61

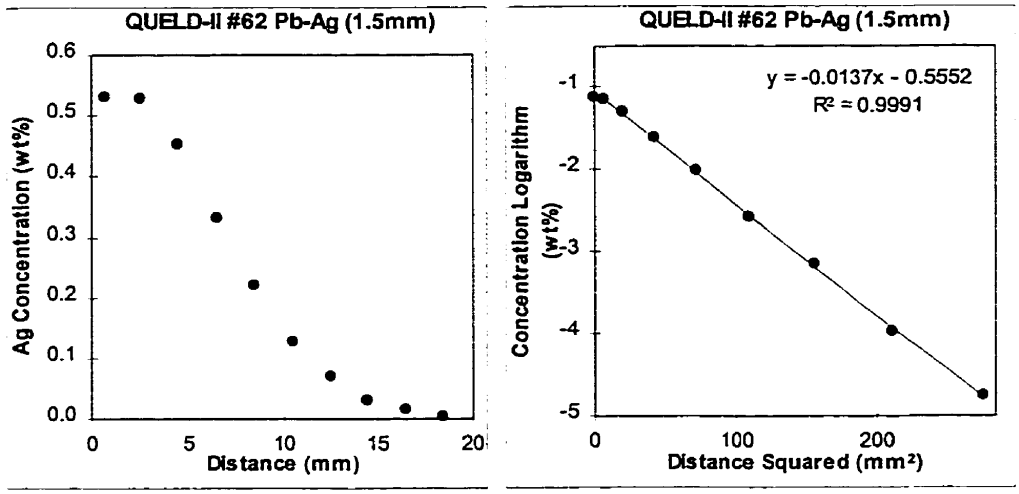

Figure IV-2 Concentration Profile and Regression Analysis of Sample #62

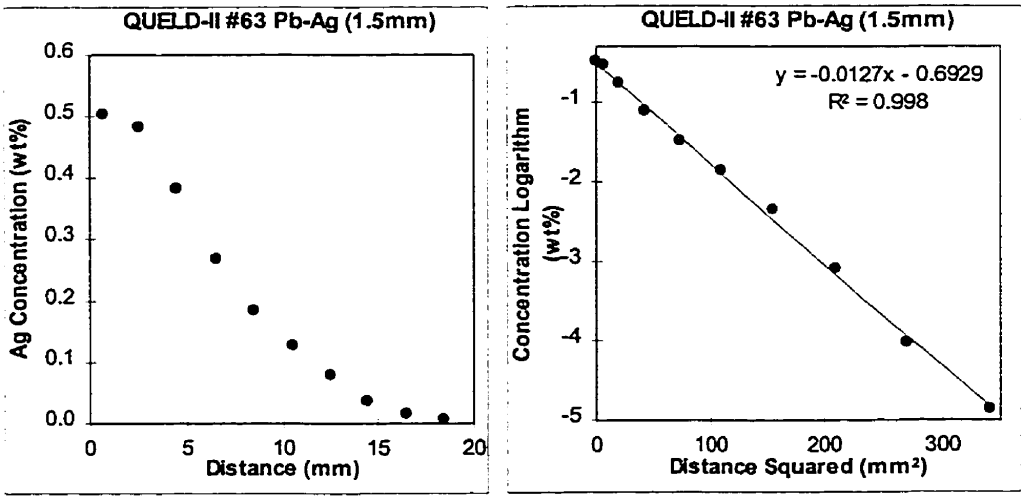

Figure IV-3 Concentration Profile and Regression Analysis of Sample #63

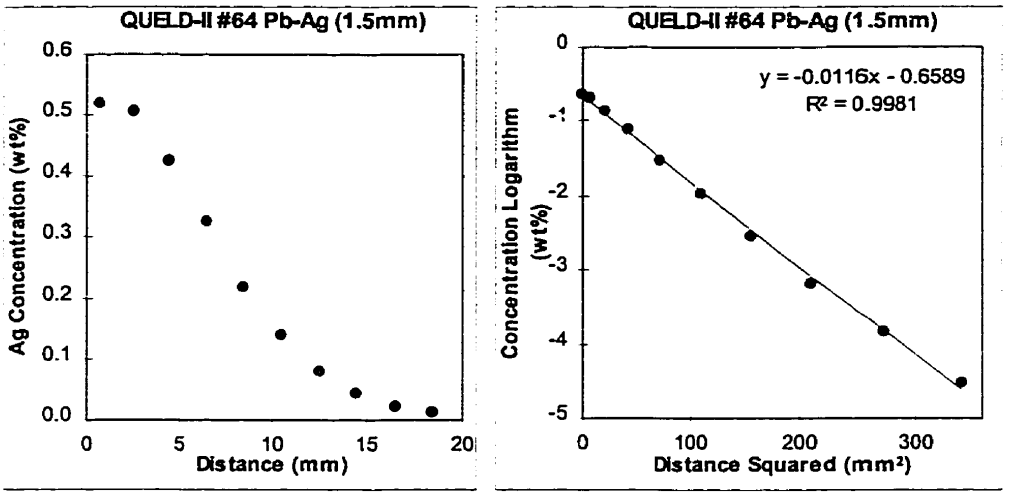

Figure IV-4 Concentration Profile and Regression Analysis of Sample #64

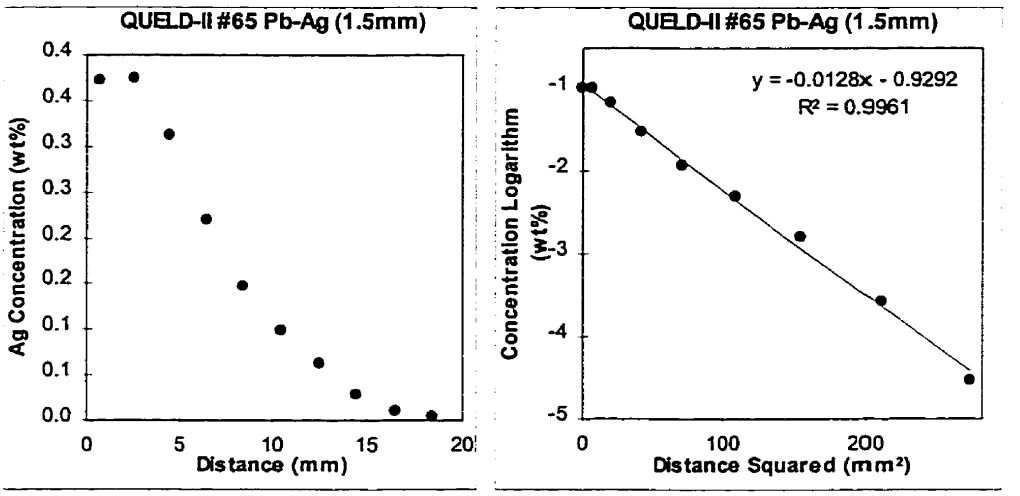

Figure IV-5 Concentration Profile and Regression Analysis of Sample #65

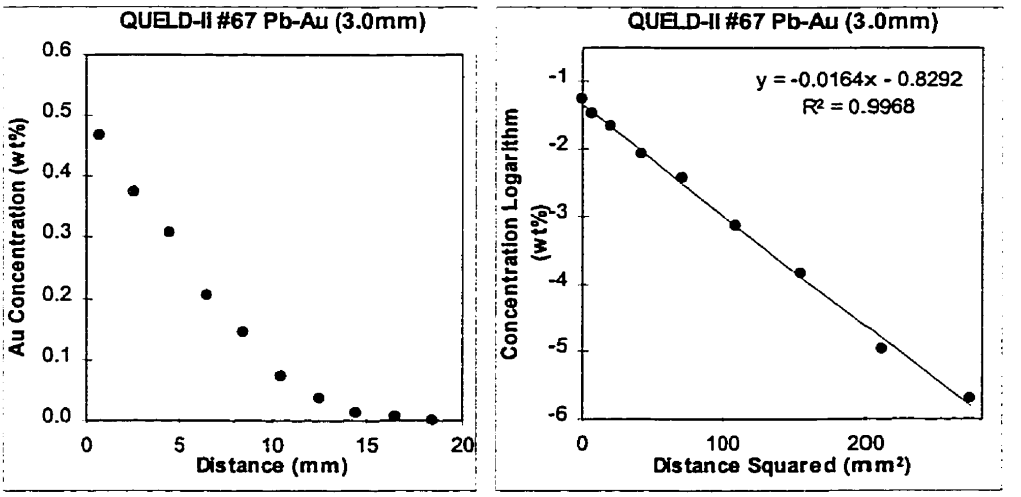

Figure IV-6 Concentration Profile and Regression Analysis of Sample #67

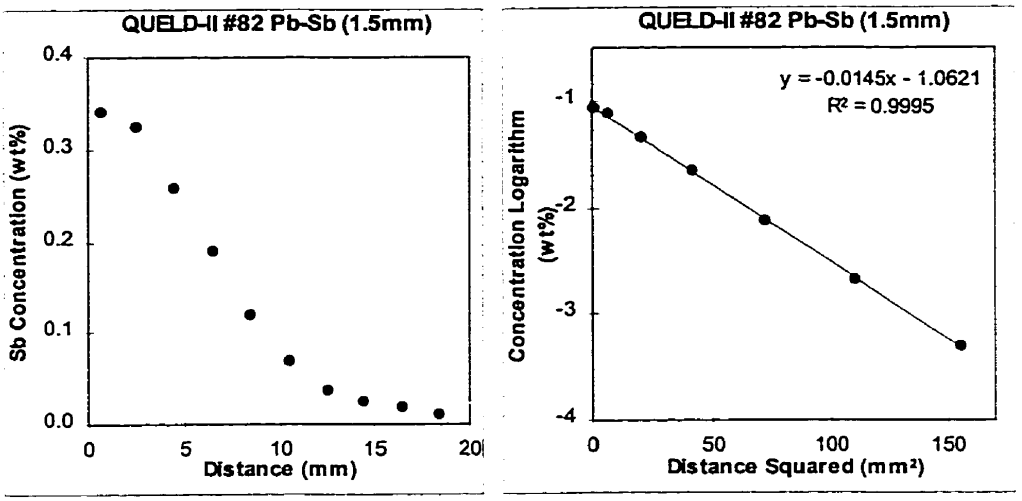

Figure IV-7 Concentration Profile and Regression Analysis of Sample #82

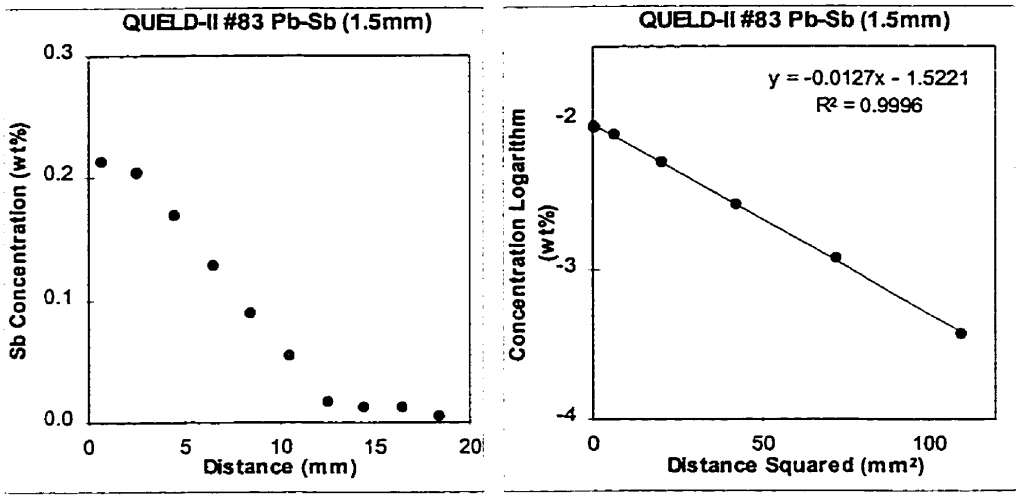

Figure IV-8 Concentration Profile and Regression Analysis of Sample #83

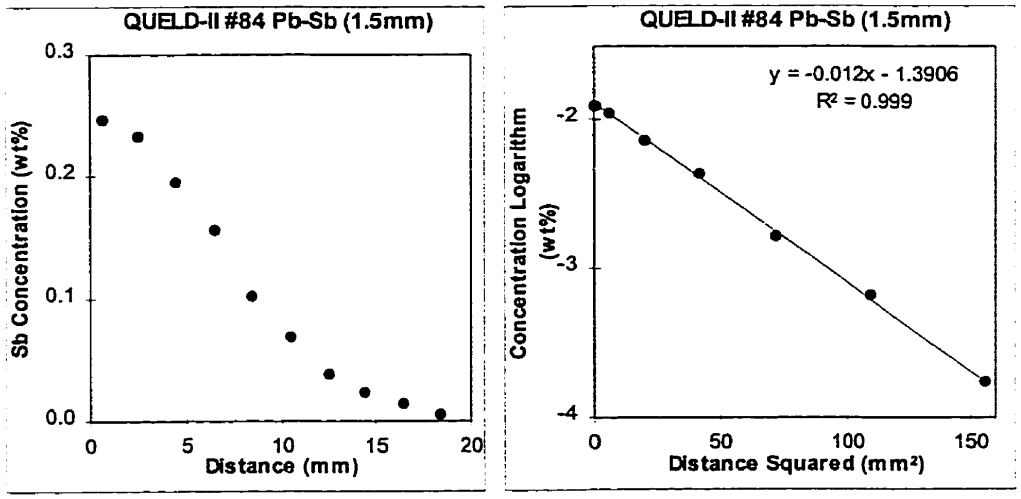

Figure IV-9 Concentration Profile and Regression Analysis of Sample #84

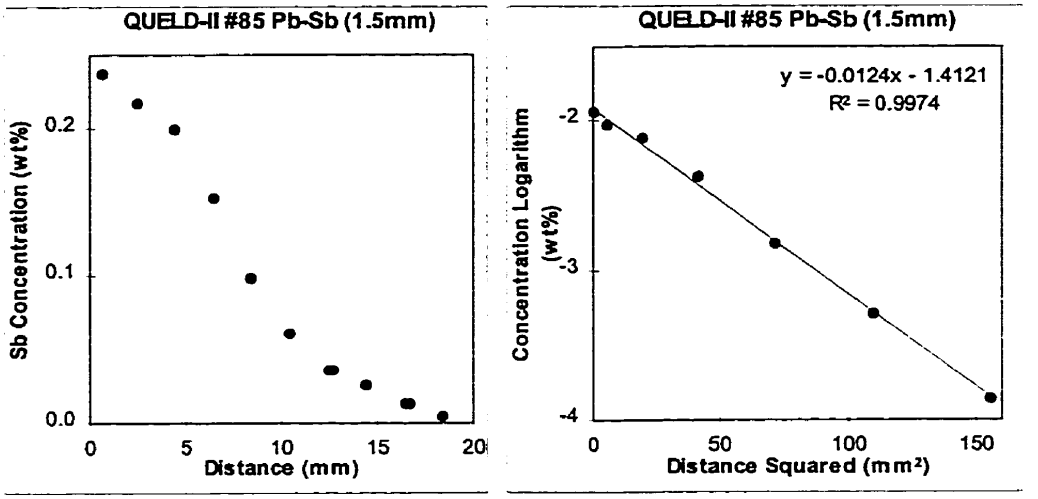

Figure IV-10 Concentration Profile and Regression Analysis of Sample #85

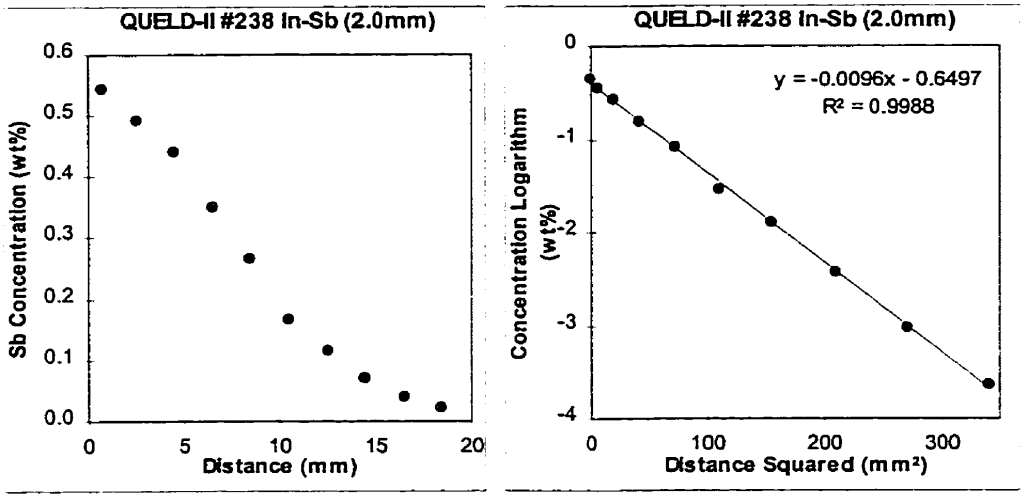

Figure IV-11 Concentration Profile and Regression Analysis of Sample #238

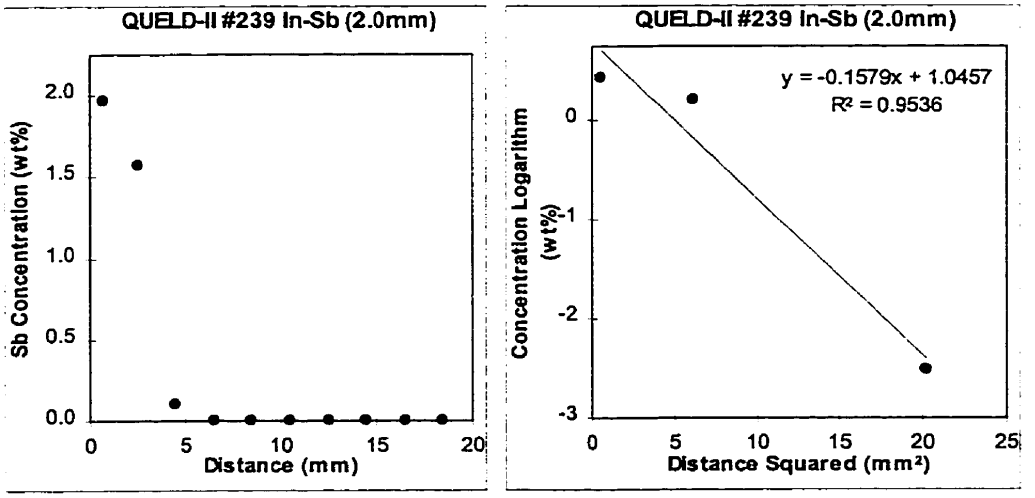

Figure IV-12 Concentration Profile and Regression Analysis of Sample #239

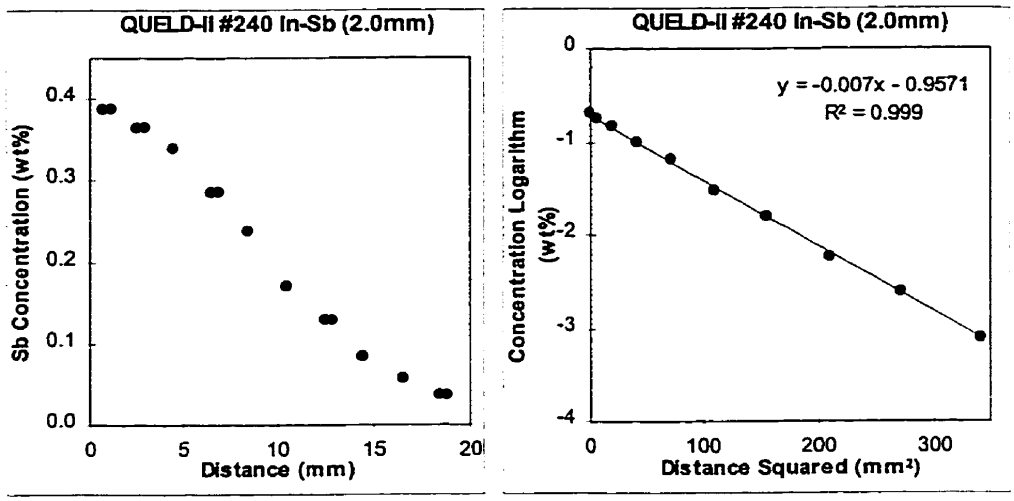

Figure IV-13 Concentration Profile and Regression Analysis of Sample #240

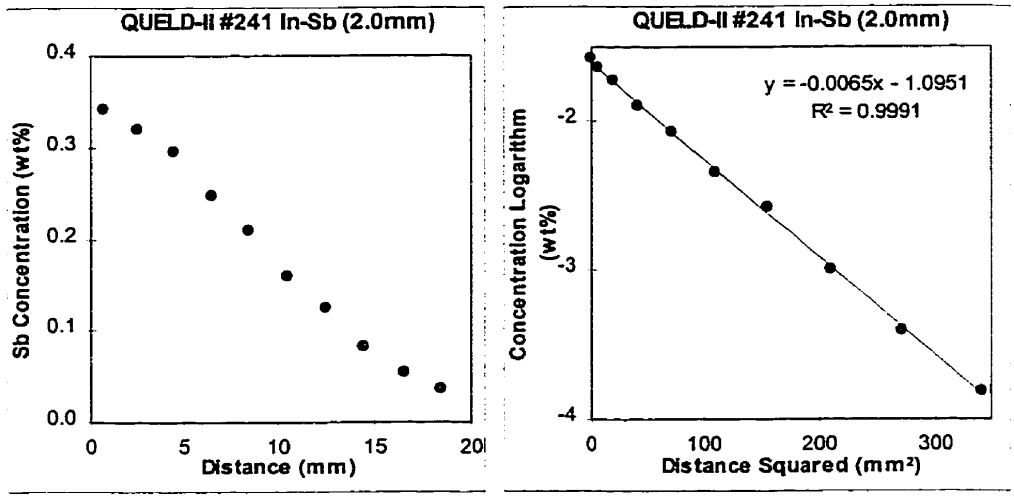

Figure IV-14 Concentration Profile and Regression Analysis of Sample #241

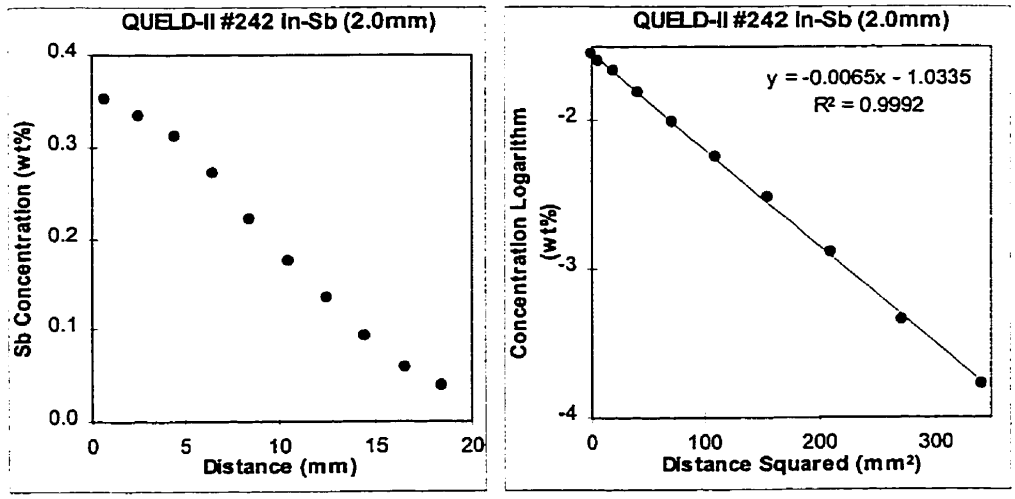

Figure IV-15 Concentration Profile and Regression Analysis of Sample #242

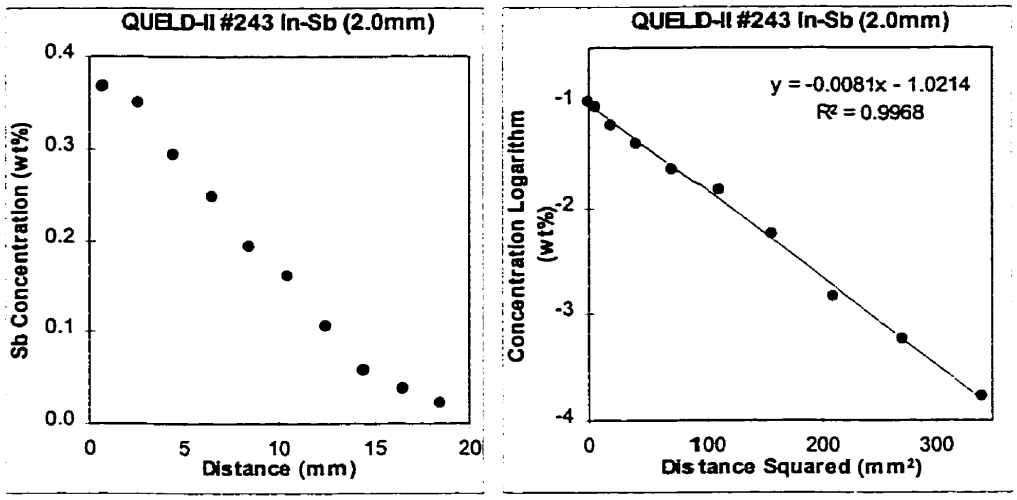

Figure IV-16 Concentration Profile and Regression Analysis of Sample #243

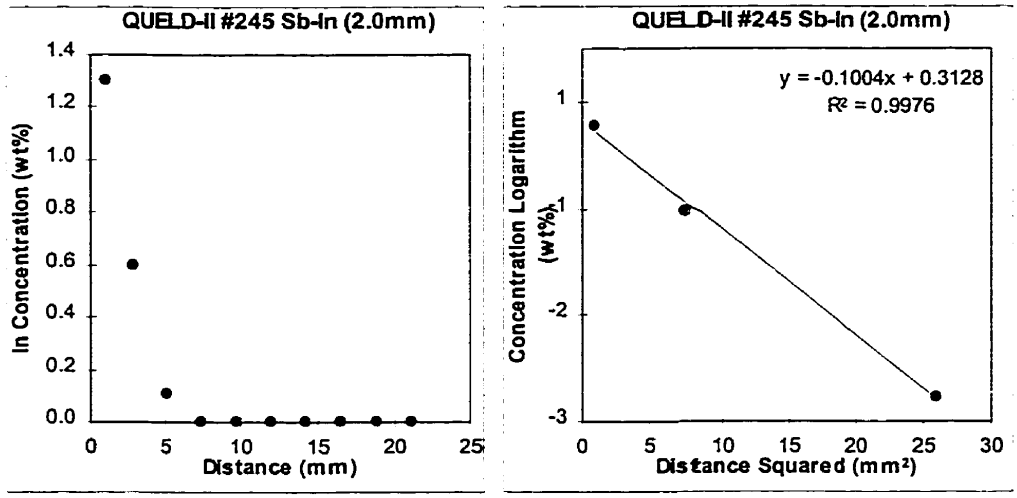

Figure IV-17 Concentration Profile and Regression Analysis of Sample #245

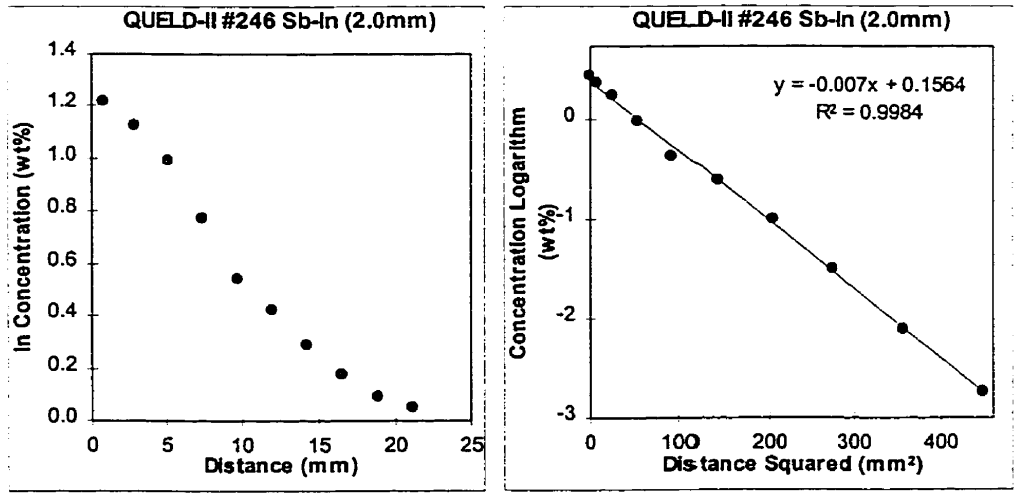

Figure IV-18 Concentration Profile and Regression Analysis of Sample #246

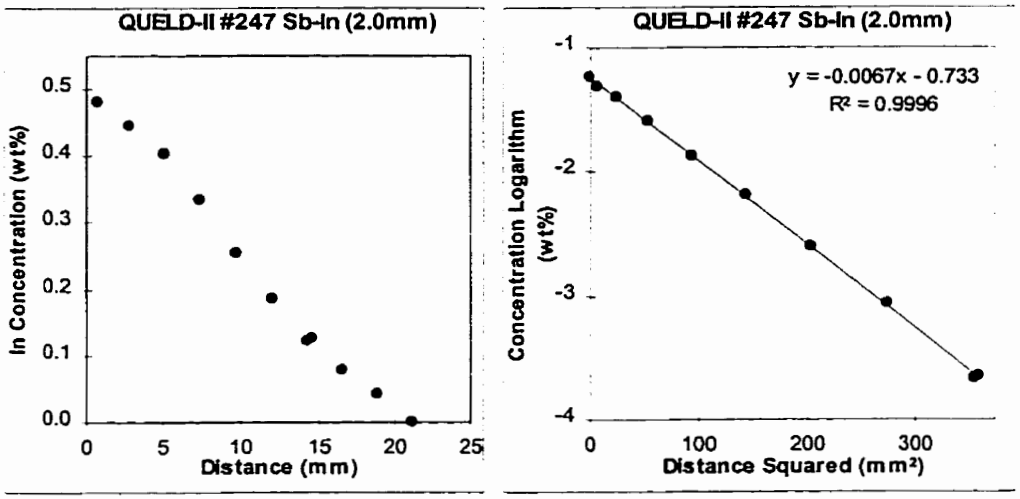

Figure IV-19 Concentration Profile and Regression Analysis of Sample #247

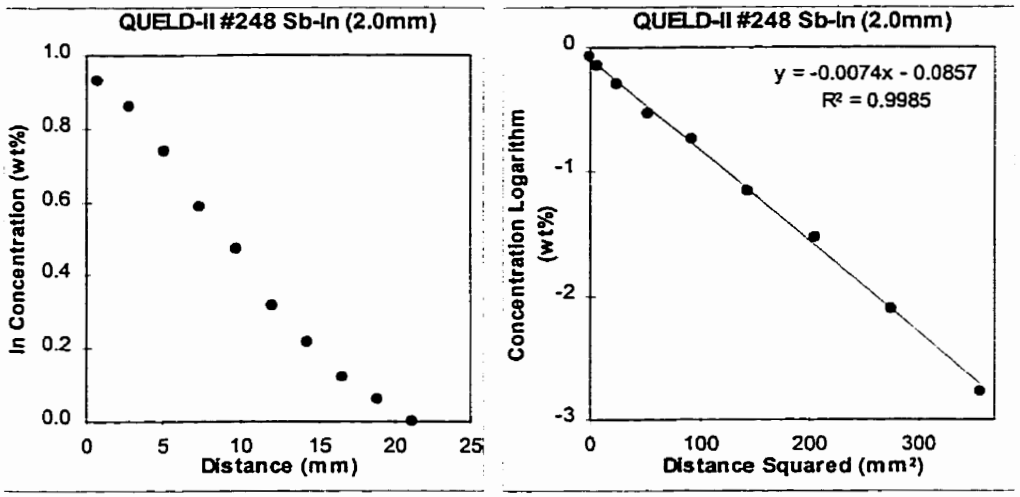

Figure IV-20 Concentration Profile and Regression Analysis of Sample #248

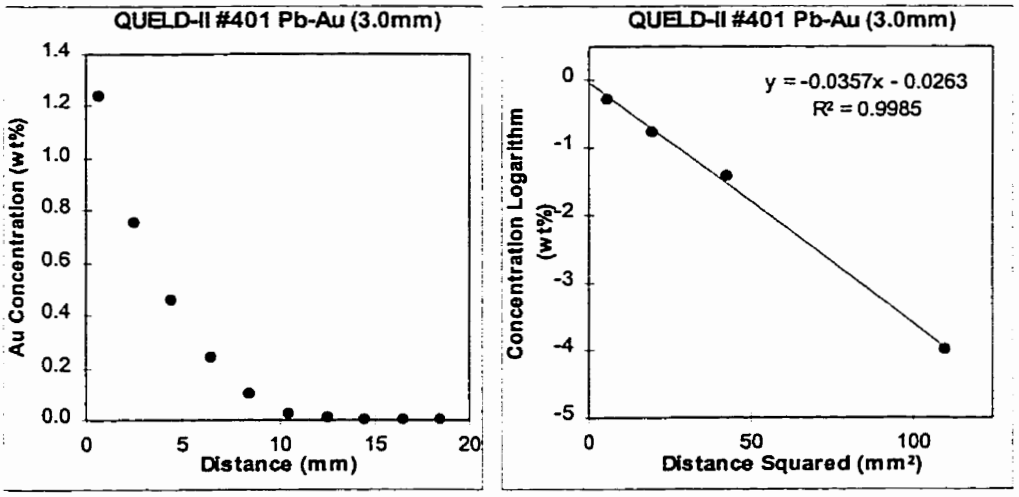

Figure IV-21 Concentration Profile and Regression Analysis of Sample #401

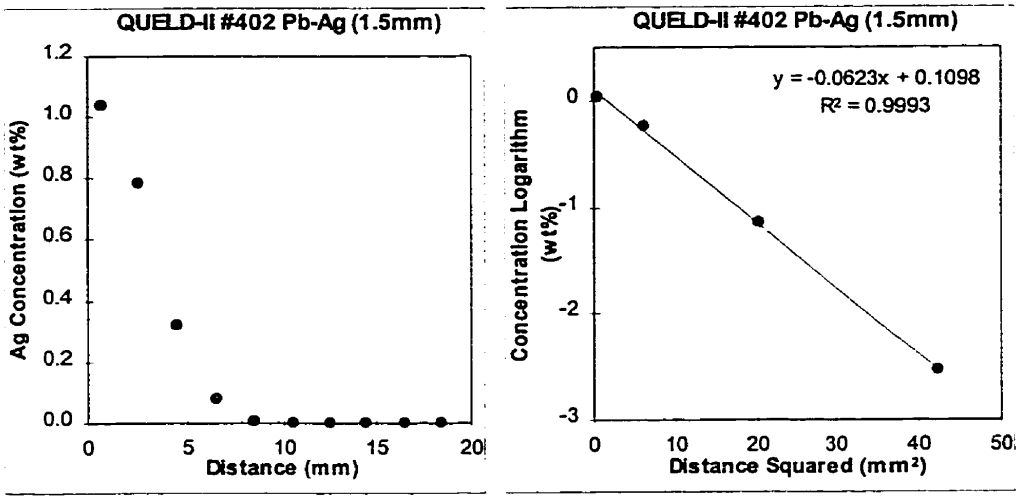

Figure IV-22 Concentration Profile and Regression Analysis of Sample #402

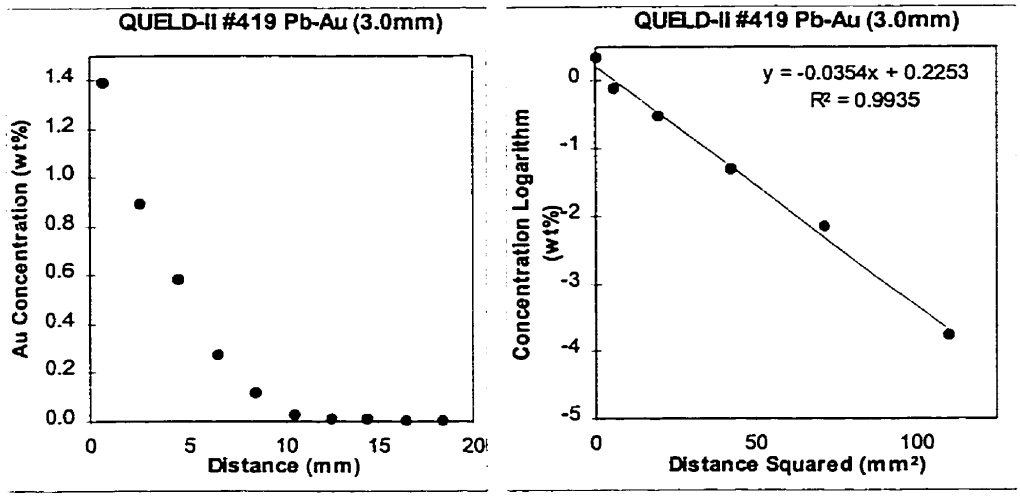

Figure IV-23 Concentration Profile and Regression Analysis of Sample #419

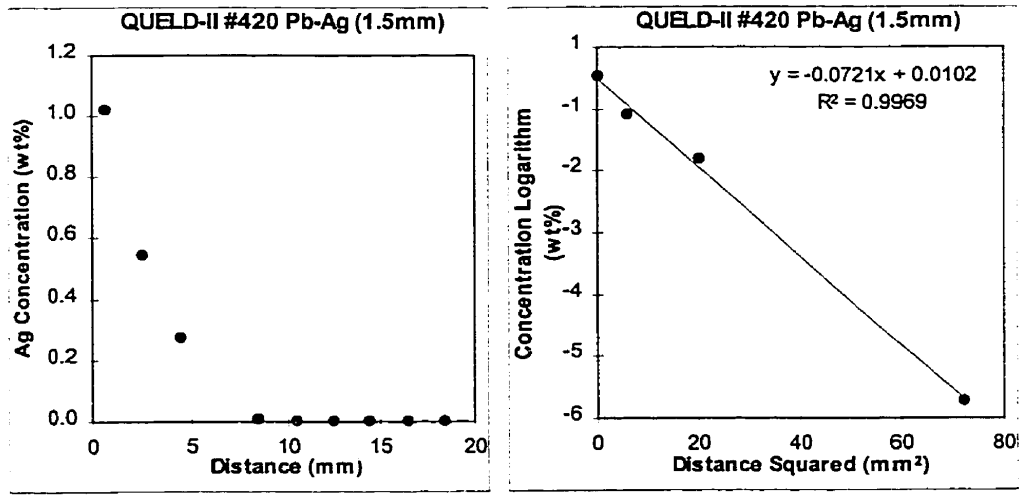

Figure IV-24 Concentration Profile and Regression Analysis of Sample #420

Table IV-1 Summary of Sample Processing Parameters and Diffusion Coefficient Results

Sample Number	System Solvent-**Solute**	MIM Mode	Diffusion-Anneal Temperature (°C)	Diffusion Time (hrs)	Diffusion Coefficient (mm^2/s) 10^{-3}
61	Pb-**Ag**	Isolated	400	1.10	3.80
62	Pb-**Ag**	Isolated	500	1.02	4.97
63	Pb-**Ag**	Isolated	600	0.93	5.88
64	Pb-**Ag**	Isolated	700	0.85	7.04
65	Pb-**Ag**	Isolated	800	0.67	8.10
67	Pb-**Au**	Isolated	600	0.83	5.10
82	Pb-**Sb**	Isolated	400	1.75	2.74
83	Pb-**Sb**	Isolated	550	1.30	4.21
84	Pb-**Sb**	Isolated	700	0.98	5.91
85	Pb-**Sb**	Isolated	800	0.83	6.75
238	In-**Sb**	Isolated	300	1.88	3.85
239	In-**Sb**	Isolated	400	1.70	0.26*
240	In-**Sb**	Isolated	500	1.52	6.53
241	In-**Sb**	Isolated	600	1.33	8.03
242	In-**Sb**	Isolated	700	1.15	9.29
245	Sb-**In**	Isolated	650	2.13	0.33*
246	Sb-**In**	Isolated	700	1.75	5.67
247	Sb-**In**	Isolated	750	1.47	7.10
248	Sb-**In**	Isolated	800	1.17	8.02
401	Pb-**Au**	Forced[1]	400	0.33	5.89
402	Pb-**Ag**	Forced[1]	400	0.33	3.38
419	Pb-**Au**	Latched[2]	400	0.33	5.94
420	Pb-**Ag**	Latched[2]	400	0.33	2.92

[1]Forced oscillations: 0.1 Hz at 45 ° to sample axis

[2]Unconfirmed MIM Data

*Irregularly Processed Sample